reviewer #1

The manuscript describes and analyses a strong episode of dust on the eastern Mediterranean region, by using satellite, surface and models for estimating the impact of dust on surface radiation. The analysis is sound and merits publication in this journal. It is also of interest for applications such as solar energy forecast. In any case, only minor comments are asked to be taken into account.

- However it would be interesting to add real measurements of solar energy plants to the estimations here described, if available.

Author's reply: The solar energy plants receive the input energy which is the local energy yield and produce the energy output which is only a percentage of the inputs because of the total system and material losses. The climatological, topographical and geographical conditions are affecting the performance as well. As a result, adding real measurements of solar energy plants is a complex issue while the comparison of RTM simulations against real plants measurements, needs a completely separate and energy-losses analysis. We agree with the reviewer that this would be interesting and we hope to have the opportunity to study real solar plant measurements in a following study.

- Page 2, lines 24-25: please state the reason to choose LibRadTran model among the different models available (if any specific reason). It would be useful to state briefly the advantages. Cite accordingly.

Author's reply: We thank the reviewer for this comment. In the revised paper we included a brief description of the advantages using libRadtran.

- Page 4, line 15: "the temporal resolution of AERONET measurements is very high (_1 per 10 minutes)". This statement is relative. AERONET performs direct AOD measurements broadly every 15 minutes. Other instruments measure the AOD every 1 minute or less. So I do not consider the temporal resolution to be very high in relation to other instruments available.

Author's reply: The sentence has been restated.

- Page 7, line 18: what is the comparison of CALIPSO and MODIS in terms of AOD for the specific episode?

Author's reply: The maximum AOD observed with CALIOP is about 3 in the center of the plume, while the corresponding AOD from MODIS is almost 3.5 over the Greek region and about 3 over the plume part that CALIPSO overpasses. We added the proposed direct comparison of these two sensors in the revised version.

5 ■ Page 8, lines 14-27: only level 2 retrievals should be used for climate data records, although level 1.5 are still useful for analysing specific cases. The authors decided to use only level 1.5 data. Do the authors consider that level 2 data criteria were too strict for this particular case, based on their experience or other simultaneous measurements? Could the authors state which AERONET criteria were decisive for not attaining level 2?

10 Author's reply: In this particular Dust Case, level 1.5 and level 2.0 AOD products had exactly the same data points. Figure 5 upper plot demonstrated both level 1.0 and level 2.0 (identical to level 1.5). The automatic filtering algorithm (described at Smirnov et al.,2000) filters out a lot of AOD values due to very rapid change of aerosol load. For AOD study we have used level 1.0 data because this high values were considered as "clouds" when in reality there were irregular high dust concentration. There is no way to have this estimation using only CIMEL measurements, so it cannot be applied in 15 AERONET algorithms or generalize this method. But the general picture of the atmospheric conditions on that particular day, described in detail in the present study, drives us to this approach. For inversions retrievals we have used level 1.5 products, although most measurements have already been filtered out by the cloud screening procedure, we just wanted to skip the sza>50º criterion used for level 2.0. We keep in mind that retrievals at sza<50º have higher uncertainties, but considering our scientific interest on that episode and the importance of having some ground based estimation of the nature 20 of aerosols we chose to proceed with level 1.5. Inversion products haven't been used in model calculations, so these higher uncertainties are not spread in our results. The paragraph has been restated to clarify the difference between AOD level 1.0 and inversions level 1.5 products.

■ Page 8, line 31-32: for the 8 year climatology, level 1.5 or level 2 was used?
25

Author's reply: The climatology was based on Level 1.5 data. This information was added in the revised version.

■ Page 7, line 8: "extends" or "is extended"

30 Author's reply: Corrected.

■ Page 7, line 18: CALIPSO - Page 8, line 30: "by comparing"?

2

Author's reply: We corrected these two grammatical failures. Thank you for noticing them.

- Page 10, line 3: please revise

Author's reply: We revised the sentence, thank you for mention this.

- Page 10, line 6: describe figure 9 before passing on figure 10

Author's reply: You are right. We corrected that.

- Page 10, line 11: perhaps I missed something, but I would say you refer to AOD instead of radiative forcing.

Author's reply: We want to thank the reviewer for the carefully reading and this conceptual correction. The reference was for the AOD indeed, so we made the appropriate revision.

- Figure 5: add axis units

Author's reply: The axis units were added in the revised paper.

- Figure 6: avoid using smoothed lines between points, as in the other figures

Author's reply: In the revised paper we used straight lines between points in Figure 6 and anywhere else it was applicable (e.g. not in mean spectrally polynomial fitting case).

- Figure 8: plot c, state UV index or units. Same for caption.

Author's reply: We thank the reviewer for this definition omission. We now fixed this issue for both plot and caption.

reviewer #2

This is a case study of a dust event that occurred in the Eastern Mediterranean during 30 January and 3 February 2015, and its impact on the solar radiation received at the surface. Used are observations from a variety of sources such as AERONET, MODIS, CALIPSO, a radiative transfer model and a chemical transport model and the 1-day ahead forecasts from the Copernicus Atmosphere Monitoring Service. It is reported that such a dust event can result in attenuation of the global radiation by as much as 40-50%, and a decrease of 80-90% in the direct component.

The approach used in this study follows methodologies implemented in numerous previous studies on the impact of dust on the reduction of solar radiation at the surface (and/or at the TOA). As such, the results obtained are to be expected. Some references to previous relevant work are included here.

▪ The actual value of the analysis to forecasting such impacts is not obvious since in real time, all the information that was available in this case in hindsight, will not be available in real time. Therefore, such impacts on solar energy planning will have to be estimated from previous knowledge of anticipated reduction.

Author's reply: The 1-day ahead CAMS aerosol forecasts can provide the basic model input information in order to predict with accuracy (within 10% as compared to the MODIS hindsight data) the AOD values in an operationally good temporal and spatial resolution (1-hour, 0.4 degrees). The other critical input is the solar zenith angle which can be pre-calculated, so the whole real time approach is feasible in terms of pre-calculated and forecasted input data to the RTM. As a result, the main output can be operational maps (like in Fig. 10) of GHI, DNI and percentage attenuation. We have now added this additional information to the text as to briefly describe the real time possibilities.

▪ Since the case was well documented with information from numerous sources (no validation at the surface was attempted), perhaps a brief communication on this case with a substantially reduced number of figures would be appropriate.

Author's reply: This dust case was the most extreme events in the last 5 years for the specific area, so we decided to not only study the energy impact which is the main scope of this paper, but to investigate from an observational point of view its intensity and characteristics. We believe that this complementary approach was highlighted throughout the text.

▪ The bibliography provided is very selective. Some relevant publications:

a. Tegen, Ina, Lacis, Andrew A., Fung, Inez Nature, 1996. The influence on climate forcing of mineral aerosols from disturbed soils. Apr 4, 380, 6573, ProQuest pg. 419.

b. Li, F, Vogelmann AM, Ramanathan V., 2004. Saharan dust aerosol radiative forcing measured from space. Journal of Climate. 17:2558-2571.

c. Diaz, J. P., F. J. Exposito, J. Torres, F. Herrera, J. M. Prospero, and M. C. Romero, 2001. Radiative properties of aerosols in Saharan dust outbreaks using ground-based and satellite data: Applications to radiative forcing. J. Geophys. Res., 106, 18 403– 18 416.

d. Haywood, J. M., P. N. Francis, M. D. Glew, and J. P. Taylor, 2001. Optical properties and direct radiative effect of Sharan dust: A case study of two Saharan dust outbreaks using aircraft data. J. Geophys. Res., 106, 18 417–18 430.

e. Kaufman, Y. J., A. Karnieli, and D. Tanre, 2000. Detection of dust over the desert by EOS-MODIS. IEEE Trans. Geosci. Remote Sens., 38, 525–531.

f. Kaufman, Y.J., D. Tanre, O. Dubovik, A. Karnieli, and L. A. Remer, 2001. Absorption of sunlight by dust as inferred from satellite and ground-based remote sensing. Geophys. Res. Lett., 28, 1479– 1482.

g. Pandithurai, G., et al., 2008. Aerosol radiative forcing during dust events over New Delhi, India, J. Geophys. Res., doi: 10.1029/2008JD009804.

h. Miller, R. L., I. Tegen, and J. Perlwitz, 2004. Surface radiative forcing by soil dust aerosols and the hydrologic cycle, J. Geophys. Res., 109, D04203, doi: 10.1029/2003JD004085.

Author's reply: We thank the reviewer for these additional references. It will be a valuable addition, so we included them in the revised paper.

- When providing information on outliers, indicate the % of total number of points available.

Author's reply: The outliers represent less than 0.5% of the data (250 points) of total coincident values. We thank the reviewer for mentioning this omission. We added this information in the revised version.

- Since the paper deals with the Eastern Mediterranean, examples of CSP installation in that region should be mentioned (instead of a facility in Western Med).

Author's reply: We added some relevant CSP installations for the Eastern Mediterranean as well since the whole Mediterranean region is often affected by Saharan dust plumes.

- Acronym and references should be provided the first time used (e.g., P. 2, L. 25: libRadtran).

Author's reply: We want to thank the reviewers for all the careful remarks. We have now corrected all the structural issues.

■ P. 3, L. 23, stated: "In this paper MODIS Aqua C6 L2 is used". There are differences between Terra and Aqua. Why Aqua was selected?

Author's reply: The present study investigates the impact of dust aerosols during an extreme dust event on surface solar radiation. In the framework of the study and in order to describe the dust event both passive and active satellite remote sensing instrumentation (MODIS and CALIOP) are utilized. Indeed the reviewer is right, the anomalously high aerosol load recorded between the 30th of January and the 3rd of February 2015 over the domain of eastern Mediterranean Sea is captured both by Aqua MODIS and Terra MODIS. There are differences between Terra and Aqua. Both Terra and Aqua are sun-synchronous, near-polar circular orbit satellites. Terra crosses in descending node the equator at approximately 10:30 A.M. local time. On the contrary, Aqua crosses in ascending node the equator at approximately 1:30 P.M. local time. Both Aqua-MODIS and Terra-MODIS spectroradiometers image the same domain on the Earth's surface with a difference of approximately three hours. The dust event, having a duration of three days, is captured well by both MODIS sensors. The selection of Aqua-MODIS in the present study is related to the orbit of Aqua which meets the needs of providing the 3-dimentional overview and description of the dust event. Aqua, being part of the A-Train constellation of earth observation satellites, flies in formation with CALIPSO. Consequently, the synergy of Aqua-MODIS and CALIPSO-CALIOP results in the horizontal and vertical description of the dust event, hence on the 3-dimensional overview. This could not have been achieved if focusing on the Terra-MODIS retrievals. For this clarification, we added the above brief description in the revised paper.

■ P. 4, L. 19, stated: "The final analysis data (FNL) of the National Center for Environmental Protection (NCEP) are used for the assessment of the meteorological conditions". Later on, on P. 4, L. 27: Stated: "COSMO-ART is a regional atmospheric model which couples online meteorology and chemistry and is used". Some explanation is needed why both are needed.

Author's reply: The FNL are meteorological reanalysis data at 1x1 resolution and are used to represent the synoptic scale conditions during this period. Also FNL is part of the GDAS data assimilation system that we used to drive the HYSPLIT runs and as seen in Figures 1a,b both datasets confirm the favorable conditions for the transport of Saharan dust towards the Aegean.

On the other hand, COSMO-ART is a more complex prognostic model and it is used for the numerical simulation of the interactions between atmospheric chemistry and meteorology at regional scale. The model solves all relevant equations at every time step (30 sec), so that the aerosol (in our case, dust particles) effects on the earth radiative budget are estimated accordingly (e.g. Figures 11 and 12).

■ P. 11, L. 28, stated: "Surprisingly, further inland in the Balkan peninsula, where the surface is less affected by the dust plume during the dust event. This means that the interaction of dust particles with the atmosphere leads to a positive feedback on solar radiation at the area north of the plume." The connection between these two statements requires clarification.

5

Author's reply: We realize that the connection between the position of the dust plume tongue and the direct radiative effects is not evident, because of the structure of the relevant paragraph. In short –and as already described in previous relevant studies (e.g. Stanelle et al., 2010), the interactions between dust aerosol and radiation creates a thermal gradient in the atmosphere, which causes a shift of the dust tongue towards the south. In other words, when the interaction is on (base-case

10 run) more amounts of direct solar radiation are received at ground further inland the Balkan peninsula, due to the aforementioned mobility of the dust plume from north to south. In order that this is clearer in the revised document, a restructuring in the relevant paragraph is performed.

■ P. 12, L.17, stated: "This study reconfirms and quantifies high dust aerosol load impact on surface solar radiation."

15 Since this study only "reconfirms" what is already known, it is recommended to condense it to a short communication.

Author's reply: We thank the reviewer for this comment in order to clarify the significance of the communication followed in this paper. Actually, by concluding in this way we wanted to "reconfirm" such quantified aerosol impacts on SSR, adding a perspective on operational energy planning using a synergy of CAMS AOD forecasts and pre-calculated inputs like the

20 SZA. This knowledge will enable the evolution of accurate near real time, nowcasting and forecasting SSR estimation models and systems as to provide already know information at the right time and not as post processing reanalysis data. At the same time, since this dust case was one of the most intense of last 5 years, it is useful for the readers to follow our proposed methodology with reference to a recent case study. As a result, we highlighted the multifaceted approach covering the model simulations from RTM and CTM in conjunction with the predicted AOD from CAMS, its validation against

25 MODIS data and the 3D observational dust plume description. We strongly believe that this study forwards the quantification of the PV and CSP losses from dust events and it will be a step to the right direction of the energy related policies.

Authors: Once again, we thank the reviewers for their constructive comments and we believe that after the proposed

30 revisions this study was overall upgraded.

Dust impact on surface solar irradiance assessed with model simulations, satellite observations and ground-based measurements

Panagiotis G. Kosmopoulos[1,2], Stelios Kazadzis[3], Michael Taylor[2], Eleni Athanasopoulou[1], Orestis Speyer[1], Panagiotis I. Raptis[1], Eleni Marinou[2,4], Emmanouil Proestakis[4,5], Stavros Solomos[4], Evangelos Gerasopoulos[1,6], Vassilis Amiridis[4], Alkiviadis Bais[2], Charalabos Kontoes[4]

[1]Institute for Environmental Research and Sustainable Development, National Observatory of Athens, Greece
[2]Laboratory of Atmospheric Physics, Aristotle University of Thessaloniki, Greece
[3]Physicalisch-Meteorologisches Observatorium Davos, World Radiation Center, Switzerland
[4]Institute for Astronomy, Astrophysics, Space Applications and Remote Sensing, National Observatory of Athens, Greece
[5]Laboratory of Atmospheric Physics, Department of Physics, University of Patras, Greece
[6]Navarino Environmental Observatory, Messenia, Greece

Correspondence to: P.G. Kosmopoulos (pkosmo@meteo.noa.gr)

Abstract. This study assesses the impact of dust on surface solar radiation focussing on an extreme dust event. For this purpose, we exploited the synergy of AERONET measurements and passive and active satellite remote sensing (MODIS and CALIPSO) observations, in conjunction with radiative transfer model (RTM) and chemical transport model (CTM) simulations and the 1-day ahead forecasts from the Copernicus Atmosphere Monitoring Service (CAMS). The area of interest is the eastern Mediterranean where anomalously high aerosol loads were recorded between the 30 January and 3 February 2015. The intensity of the event was extremely high, with aerosol optical depth (AOD) reaching 3.5, and optical/microphysical properties suggesting aged dust. RTM and CTM simulations were able to quantify the extent of dust impact on surface irradiances and reveal substantial reduction in solar energy exploitation capacity of PV and CSP installations, under this high aerosol load. We found that such an extreme dust event can result to Global Horizontal Irradiance (GHI) attenuation by as much as 40-50%, a much stronger Direct Normal Irradiance (DNI) decrease (80-90%), while spectrally this attenuation is distributed to 37% in the UV region, 33% to the visible and around 30% to the infrared. CAMS forecasts provided a reliable available energy assessment (accuracy within 10% of that obtained from MODIS). Spatially, the dust plume resulted in a zonally-averaged reduction of GHI and DNI of the order of 150W/m^2 in southern Greece, and a mean increase of 20 W/m^2 in the northern Greece as a result of lower AOD values combined with local atmospheric processes. This analysis of a real-world scenario contributes to the understanding and quantification of impact range of high aerosol loads on solar energy and the potential for forecasting power generation failures at sunshine-privileged locations where solar power plants exist, are under construction, or being planned.

1 Introduction

Solar energy potential is sensitive to various atmospheric parameters. In addition to the solar zenith angle (SZA) as the key determining factor, cloud presence is another factor that attenuates solar radiation arriving at the Earth's surface. For this, large photovoltaic (PV) installations are built where solar insolation is high and cloud-free sky conditions prevail for the largest part of the year. However, in the case of European sponsored installations, these are also significantly affected by mineral dust, mainly perimetrically of the Western (e.g. the 160 MW Noor Concentrated Solar Power (CSP) in Morocco) and Eastern (e.g. the 150 MW Kuraymat CSP in Egypt and the 130 MW Ashalim CSP in Israel) Mediterranean (e.g. the 160 MW Noor Concentrated Solar Power (CSP) in Morocco).

The aerosol radiative effects over the eastern Mediterranean have been studied systematically in the last decade (e.g. Papadimas et al., 2012; Turnock et al., 2015; Lindfors et al., 2013). It is a semi-enclosed sea surrounded by continental area with discrete sources of aerosols and it is characterized by large direct radiative effects due to high and frequently dust loads, especially during spring (Kosmopoulos et al., 2008; Gkikas et al., 2012; 2013; Flaounas et al., 2015; Athanasopoulou et al., 2016). A recent climatology of global aerosol mixtures, derived from 7 years GOCART model simulations (Taylor et al., 2015), suggests that dust is the primary component of aerosol mixtures over the eastern Mediterranean. While the spatial extent of dust mixtures is fairly stable on the seasonal timescale, they are highly variable in time at the local scale. Desert dust plays an important role in the radiative forcing (RF), with an estimated Top of Atmosphere (TOA) RF in the range of -0.6 to 0.5 W/m^2 (IPCC, 2013), and at the ground is -0.96 W/m^2 (Tegen et al., 1996). Still, dust induced RF is very uncertain in both magnitude and sign, an uncertainty driven by the chemical composition of mineral particles (Claquin et al., 1998), the wavelength dependence of their optical properties (e.g. single-scattering albedo -SSA-, asymmetry factor) as well as the albedo of the underlying surface and the relative height between the dust layer and the clouds (Kaufman et al., 2001; Kinne and Pueschel, 2001; Pandithurai et al., 2008).

In the absence of clouds, dust is the main source of attenuation of the surface solar radiation (SSR), with the direct normal irradiance (DNI) being affected much more intensively than the global horizontal irradiance (GHI). Many studies focus on different approaches to quantify and estimate the impact of dust on the SSR (Dirnberger et al., 2015; Ishii et al., 2013; Lindfors et al., 2013; Allen et al., 2013; Qian et al., 2007; Papayiannis et al., 2005). In order to assess the impact of strong dust events on solar energy, a monthly climatology of aerosol optical depth (AOD) and spectrally-integrated SSR, including the direct normal irradiance (DNI) and the global horizontal irradiance (GHI), was calculated with the radiative transfer model (RTM) libRadtran (Mayer & Kylling, 2005). LibRadtran contains a library of radiative transfer routines, which, advantageously on other models (Emde and Mayer, 2007; Cahala, et al., 2005; Marquart and Mayer, 2002), were originally designed to calculate spectral irradiance in the ultraviolet and visible spectral ranges. Is user friendly, since it allows the definition of the RTM inputs with human-readable files, and finds applications in simulation of instruments, calculation of the radiation budget of the Earth and, as in this study, in the development of remote sensing techniques. The present study computes the direct effect of the extreme dust event of the 1 February 2015 on the radiative energy budget using satellite and

ground-based data as input to the RTM. The study area covers the eastern Mediterranean and more specifically the region of Greece. Dust cases in winter are rare, but intense when they occur (Gerasopoulos et al., 2011; Kosmopoulos et al., 2011), thus the study of such an event is of great interest with respect to low incoming SSR and the typical winter meteorological conditions. In order to better understand this effect, we used data from different sources to perform a multi-model analysis of

5   the intense incursion of Saharan dust into South-Eastern Europe during the study period that began with cyclonogenesis to the North of Libya on 28/01/2015, peaked over the Mediterranean on the 01/02/2015 and dissipated a couple of days later. The data synergy is provided by i) RTM simulations from libRadtran, ii) chemical transport model (CTM) simulations from COSMO-ART, iii) satellite aerosol retrievals from the MODIS spectroradiometer, iv) aerosol profiling from CALIPSO, v) aerosol retrievals provided by AERONET sunphotometers and their inversion algorithm and finally, vi) aerosol product

10   retrievals from the CAMS. We measure the attenuation of SSR during the course of the evolution of the dust outbreak and correlate it with the available data (e.g. CAMS against MODIS) to assess the relative impact of dust aerosol on solar power over the study area. The work is organized as follows: in Sect. 2 the measurements and models used are presented; then the results from the 3D observation and ground-based dimension of the dust event evolution, together with the impacts on surface solar radiation are presented in Sect. 3; finally, the conclusions are provided in Sect. 4.

15   ## 2 Measurements & Models

2.1 Measurements

2.1.1 MODIS and CALIPSO

The MODerate resolution Imaging Spectroradiometer (MODIS) sensors are among the primary instruments onboard the polar orbit sun-synchronous NASA satellites Terra and Aqua (Salomonson et al., 1989). MODIS sensors provide retrievals

20   of AOD at 550nm since February 2000 and June 2002 for Terra and Aqua satellites respectively. The retrievals of MODIS sensors are established against different types of earth surface, based on a pair of complementary algorithms, the "Dark Target" (DT) and "Deep Blue" (DB). The DT algorithm is used over vegetated/dark land surfaces which are characterized by low reflectance and additionally over ocean, while the DB algorithm provides AOD retrievals over bright and arid land surfaces (Levy et al., 2013). The accuracy of Collection 6 (C6) MODIS DT algorithm is approximately equal to $\pm$ (0.05 +

25   0.15τ_A) and + (0.04 + 0.1 τ_A), - (0.02 + 0.1 τ_A) over land and oceanic surfaces respectively, while the expected error of DB algorithm is estimated at $\pm$ (0.03 + 0.2 τ_M) (Levy et al., 2013; Sayer et al., 2015; Georgoulias et al., 2016). The input parameters τ_A and τ_M at the error estimation of the two algorithms correspond to the AOD derived by AERONET and MODIS respectively. The products of MODIS are provided in different levels of processing. The spatial resolution of MODIS Level 2 (L2) is approximately 10 km x 10 km at nadir viewing geometry, while grids are increasing significantly

30   with increasing viewing angle. In this paper MODIS Aqua C6 L2 is used and in addition to the AOD_{550nm} the Cloud Fraction (CF) over land, ocean and the DB CF over land are combined to provide the full information on the cloud coverage during

the Aqua overpass (Platnick et al., 2016). The orbit of Aqua meets the needs of providing the 3-dimentional overview and description of the dust event. Aqua, being part of the A-Train constellation of earth observation satellites, flies in formation with CALIPSO. Consequently, the synergy of Aqua-MODIS and CALIPSO-CALIOP results in the horizontal and vertical description of the dust event, hence on the 3-dimensional overview.

For the vertical distribution and structure of the atmosphere the synergy of MODIS and CALIOP (Cloud Aerosol Lidar with Orthogonal Polarization) can provide a unique 3-dimensional characterization of dust outflows (Gkikas et al., 2016; Kosmopoulos et al. 2011). CALIOP, the main instrument onboard CALIPSO (Cloud-Aerosol Lidar and Infrared Pathfinder Satellite Observations), provides information on the vertical distribution of aerosols and clouds (Winker et al., 2009) since June 2006. CALIPSO, the NASA-CNES collaboration project, is part of the A-Train constellation and therefore observes the same atmospheric layer as MODIS/Aqua at nadir viewing, with a delay of a few seconds only. CALIPSO main products include the total attenuation backscatter coefficient, at both 532nm and 1064nm, and polarization retrievals at 532nm. Based on the backscatter coefficient, the depolarization ratio, the altitude of the atmospheric layers and the surface characteristics below the orbit of CALIPSO, the CALIOP algorithm (Omar et al., 2009; Omar et al., 2016) classifies the atmospheric masses among different feature types (clear air, cloud, aerosol, stratospheric feature, surface, subsurface or totally attenuated). In the case of aerosols, the algorithm further discriminates the atmospheric layers between marine, dust, clean continental, polluted continental/smoke, polluted dust elevated smoke, dusty marine, PSC aerosol, volcanic ash and sulfate/other. In this work, the CALIPSO Level 2 Version 4.10 aerosol profile product is used.

2.1.2 AERONET

The AERONET measurements reported in this work were conducted at Thisio AERONET station (ATHENS-NOA), which is located in the capital of Greece, Athens, with a CIMEL sunphotometer (CE318). The instrumentation, data acquisition, retrieval algorithms and calibration procedure conform with the standards of the AERONET and are described in detail in numerous studies (e.g. Holben et al., 2001; Dubovik et al., 2000). Typically, the total uncertainty in AOD for the field instrument under cloud-free conditions, is ±0.01 for λ>440 nm, and ±0.02 for shorter wavelengths. In this study, the hourly-averaged data, which are cloud-screened and quality assured (Smirnov et al., 2000), were used. The temporal resolution of AERONET AOD measurements is about 4 measurements per hour in cloud free conditions. The temporal resolution of AERONET AOD measurements is very high (~ 1 per 10 minutes).

2.2 Models

2.2.1 Meteorology and back-trajectories

The final analysis data (FNL) of the National Center for Environmental Protection (NCEP) are used for the assessment of the meteorological conditions related to the uplift and transport of dust. The NCEP-FNL (Final Analysis) data are on 1°×1° grid and are available every six hours (NCEP 2000). The analyses include meteorological parameters (pressure, geopotential

height, temperature, wind etc.) inside the boundary layer, at the surface and at 26 pressure levels from 1000 hPa to 10 hPa. The HYSPLIT dispersion model (Stein et al., 2015) is used for the computation of air mass back-trajectories during the dust episode. The trajectories are calculated from 500 – 2000 m every 500 m over the Aegean Sea in order to define the transport paths of dust originally elevated at the coastal sources of N. Africa. HYSPLIT model is driven by NCEP-GDAS (FNL is also part of the GDAS and hence controls HYSPLIT's output accuracy) meteorological data at 1°×1° resolution (NCEP 2000).

2.2.2 COSMO-ART simulations

COSMO-ART is a regional atmospheric model which couples online meteorology and chemistry. COSMO is the operational numerical weather prediction model of the German and other European weather services (Baldauf et al., 2011) and is used as a regional climate model in a modified version CCLM (Rockel et al., 2008). ART (Aerosols and Reactive Trace gases) is the chemistry extension of COSMO. Detailed description of the model, of the physico-chemical characteristics of the aerosol modes and of the parameterizations of feedbacks of aerosols on radiation, temperature, cloud and ice condensation nuclei (CCN and IN) are given in Vogel et al. (2009), Bangert et al. (2011; 2012), and Rieger et al. (2014). The model domain used in this study is defined so that it includes the area of the dust source (NW Africa) and its transport path towards SE Mediterranean (from 24° to 42° N and from 5° W to 32° E). The horizontal spatial resolution is 0.25°, while the vertical extent reaches 22.7 km, stratified in 40 layers. The meteorological initialization is performed using inputs from the ICON general circulation model (Zängl et al., 2015), i.e. from the operational model runs of the German Weather Service. Anthropogenic emissions are derived from the TNO-MACC III database (Kuenen et al., 2014), while the African dust emissions are calculated online, thus are case specific. Their hourly emission rate is parameterized according to the saltation processes, as a function of friction velocity (when greater than a threshold), soil water content, and surface roughness. More information on the exact methodology can be found in Vogel et al. (2006). Apart from the base-case run, a scenario with the online interaction between dust and radiation switched off is also performed.

2.2.3 RTM simulations

For the RTM simulations we used libRadtran (Mayer & Kylling, 2005) in order to produce gridded GHI, DNI, VIS and UV spectral irradiances and integrated values at the surface with the impact of dust as well as for clean (aerosol-free) and clear (cloud-free) sky conditions. The RTM simulations convert the satellite and ground-based cloud and aerosol products directly into high resolution (1nm) spectral irradiances (Emde et al., 2016). The main input is the AOD as to quantify the exact impact of the dust particles in local (Athens) and regional (Greece) level. Other basic input parameters to the RTM simulations were the SZA, total ozone, reflectivity of the earth's surface and water vapor column. Thus, the RTM has been applied to MODIS Level 3 AOD (550 nm) data with the spatial resolution of 1x1 degree and to CAMS 1-day ahead AOD (550 nm) forecast to produce gridded spectra and spectrally-integrated total SSR values. The AERONET AOD data in the station of Athens were also used as inputs to the RTM to quantify the impact of dust on SSR. The simulated SSR values using satellite and ground-based aerosol optical properties means that this approach covers all the recognized available

aerosol data sources and the RTM outputs that could potentially be used for the proper assessment and corrections of solar power operational loads (Kosmopoulos et al., 2015).

When modeling clear (from clouds) but not clean (from aerosols) sky conditions, aerosol has a particularly important impact on the radiation budget (Schwartz et al., 2014) and hence the AOD, the Angstrom Exponent and the single scattering albedo (SSA) are included in the RTM simulations. The output wavelength range of the radiative fluxes is 285 - 2800 nm in order to facilitate an investigation into the dependence of the irradiance spectrum on particular aerosol parameters for this specific dust case and at the same time to quantify the energy potential. Furthermore, in our RTM simulations, we used the default aerosol model according to Shettle (1989), the code for spectral irradiance (COSI) developed in 1-Direction for the extraterrestrial solar source spectrum, the parameterization of molecular bands provided by LOWTRAN for the gas absorption, and finally the SDISORT radiative transfer solver (Dahlback & Stamnes, 1991), which is appropriate for large SZAs making the simulated spectra outputs valid from 0° to 90°. The RTM simulations were calculated using a band parameterization method based on the correlated-k approximation (Kato et al., 1999) and the exponential sum fitting technique. This method has been found to be able to offer accurate estimates of the spectral irradiance in spectral intervals comparable with those provided by detailed line-by-line calculations in clear and cloudy sky conditions (Nyamsi et al., 2014).

2.2.4 CAMS

Forecast data (1-day-ahead) from Copernicus Atmospheric Monitoring Service (CAMS), based on Monitoring Atmospheric Composition and Climate (MACC) reanalysis tools, were used to provide deeper understanding of the dust transport of the event and also to visualise the plume of dust aerosols. The CAMS data set includes modelling of aerosol and satellite data assimilation. The modelling part is based on ECMWF physical parameterizations concerning aerosol processes and mainly follows the aerosol treatment in the LOA/LMD-Z model (Boucher et al., 2002; Reddy et al., 2005). Detailed description of the model can be found in Morcrette et al. (2009) and Benedetti et al. (2009). In brief, it estimates dust particles emissions from 10-m wind, soil moisture, albedo in the UV-visible region and land coverage (Morcrette et al., 2008), sea-salt emissions are calculated using a source function (Guelle et al., 2001; Schulz et al., 2004), and other aerosol types emitted by domestic, industrial and transport activities are extracted from SPEW (Speciated Particulate Emission Wizard), and EDGAR (Emission Database for Global Atmospheric Research) annual- or monthly-mean climatologies (Dentener et al., 2006). Removing aerosols from the atmosphere includes wet and dry decomposition and gravitational settling, and standard schemes for all three of them are used in the model. MODIS AOD at 550nm data are assimilated into a database, applying a bias correction, which uses all available information to determine consistent bias estimates from multiple data sources (Dee and Uppala, 2009). The coupling of these data, provide a database from 2012 at 1hour time steps at 0.4ºX 0.4º spatial resolution.

13

3 Results

3.1 Synoptic description of the dust event

As seen in Fig. 1, the establishment of a cold trough during 31 January – 1 February 2015 over West Europe favors the formation of a low pressure system at the Gulf of Genoa. The mean sea level pressure (mslp) reaches 986 hPa over Corsica at 12:00 UTC, 31 January 2015 (Fig. 1a). As the system propagates towards Italy and the Balkans, frontal activity along the North Africa coastline results in increased near surface wind speeds at this area (color scale). Especially over the dust source areas located between the Gulf of Gabes in Tunis and the Gulf of Sirte in Libya, wind speeds at 1000 hPa exceed 15 m s^{-1} and dust particles mobilized are transported over the Mediterranean at the warm sector of the cyclone. The back-trajectories arriving over the Aegean Sea pinpoint to the dust sources as evident by the HYSPLIT 30-hour in Fig. 1b. The air masses arriving at heights 0-2 km over the Aegean Sea at 12:00 UTC, 1 February 2015 originate from Tunis and Libya and are embedded in the cyclonic circulation.

3.2 3-D observation

Figure 2 shows the spatial and temporal evolution of the true color imagery (a), cloud fraction (b) and AOD (c) on the days before (top), during (centre) and after (bottom) the peak of the dust event on 01 February 2015. To present the horizontal distributions of MODIS parameters the domain of the eastern Mediterranean Sea is divided into grids of spatial resolution 0.1^{o}x0.1^{o} deg each, and accordingly the closest MODIS retrieval is assigned to each grid. Note that the days before and after the dust peak were extensively cloud covered (the relationship between AOD and cloud fraction (CF) is described by many researchers e.g. Grandley et al., 2013). Elevated values of AOD (1-3) were observed up to 3 days prior and after the peak (not shown). Based on Fig. 2c centre panel, the dust plume is extendeds dramatically in the horizontal eventually reaching the Black Sea region with AOD values of similar order but with different lateral characteristics as we will discuss in the following Sect. 3.4.2. An increase of AOD from the west to the east is observed, reaching maximum values over south Greece. The dust plume yields AOD$_{550nm}$ values larger than 1, while values as high as 3 are persistently evident in the center of the plume. A decreasing gradient to the northeast is also present along the dust plume. Over the larger domain of the western Turkey the high CF and the absence of AOD$_{550nm}$ values prevent the retrieval of the horizontal evolution of the dust plume over Turkey.

Figure 3 shows the 3-D profiling of the dust plume (see Amiridis et al., 2009; 2015; Kosmopoulos et al., 2014; Mamouri et al., 2016). The horizontal distribution is provided by MODIS/Aqua C6 L2 AOD$_{550nm}$ (Left panel) while CALIPSO provides the extinction coefficient profiles at 532nm (Upper Right) and the aerosol subtype classification (Lower Right). The total effect of integrated AOD profile from CALPIPSO as input to the RTM simulations, in terms of SSR output sensitivity and effectiveness in solar energy exploitation, is similar at surface (±5%) compared to the total AOD from MODIS observations (Kosmopoulos et al., 2014), thus in all RTM simulation cases we used as input the total AOD values from MODIS and CAMS (Sect. 3.4.1). For the specific dust episode, the maximum AOD observed with CALIOP is about 3 in the center of the

plume, while the corresponding AOD from MODIS is almost 3.5 over the Greek region and 3 over the plume part that CALIPSO overpasses. At the same time, the laser backscatter signal of CALIOP becomes totally attenuated at particulate column optical depths of ~3, while for higher optical depths cannot measure the full extent of the vertical column (Vaughan et al., 2009). The plume consists mainly of dust aerosol, and polluted dust and dusty marine at the edges, in agreement with similar studies (Gkikas et al., 2016; Papayiannis et al., 2005; Li et al., 2004). Based on the CALIPSO backscatter coefficient and the depolarization ratio (532 nm) profiles, it is possible to decouple the pure dust component from the polluted dust and dusty marine mixtures, hence to estimate the dust contribution to the total AOD (Tesche et al., 2009). According to CALIPSO the contribution of dust AOD to the total AOD gradually increases from 70% to the south of the dust plume to 100% in the region between 34° and 39.5^o latitude. The dust plume extends vertically as high as 3.5 km above sea level. At the edge of the plume (31° N to 33° N), extinction coefficient values at 532 nm are around 0.2 km^{-1}, while in the center of the plume (35° N to 40° N), the lidar signal is totally attenuated bellow 1 km. The aerosol extinction coefficient at 532 nm increases from 0.2 km^{-1} at the top of the dust layer, to 2 km^{-1} at about 1.5 km distance from the top of the layer and it reached values of 10 km^{-1} just before the signal is significantly attenuated. These observations are similar with the radiative properties and the corresponding heights of desert dust aerosol measured and calculated by Haywood et al. (2001) and Hess et al. (1998).

3.3 Ground-based aerosol data

In order to provide a context for the high AOD values observed in the region during the extreme dust incursion on the 1st of February 2015, Fig. 4 presents scatter plots obtained from the multi-sensor aerosol products sampling system (MAPSS: https://giovanni.gsfc.nasa.gov/mapss_explorer/) (Petrenko et al., 2012) of the MODIS/Aqua satellite AOD at 550nm versus coincident ground-based AOD measured by CIMEL sunphotometers in AERONET (Holben et al., 1998). The data presented are outlier-free (the percentage of the outliers represent less than 0.5% of the data (250 points) of total coincident values), spanning the five-year period: 2006-2010 (inclusive) for the entire global record (≈ 50K coincident values) together with the local record at the ATHENS-NOA site (≈ 150 values). The CIMEL at the Athens site has been in operation since 07/04/2008 and provides spectral AOD data at Levels 1.0 (1993 days), 1.5 (1870 days) and 2.0 (1514 days). The coefficient of determination between the satellite and ground-based AOD is high $0.63 \le R^2 \le 0.64$ for Athens (and very high globally: $0.80 \le R^2 \le 0.81$) for both satellite sensors and reflects low root mean-squared errors ($0.07 \le RMSE \le 0.09$). In all cases, a strong high frequency of occurrence peak is apparent in the range $0 \le AOD \le 0.4$. This peak is associated with a modal value of AOD (≈0.16 globally and ≈0.13 for Athens). The extreme dust incursion event on the 1 February 2015 is therefore expected to load the aerosol optical depth over the ATHENS-NOA site and be clearly distinguishable from the baseline value of ≈0.13.

AERONET ground-based retrieval of Level 1.0 (Version 2) AOD from ATHENS-NOA site, provides approximately hourly records that enable tracing the temporal evolution of the aerosol load (Fig. 5). Values reach up to 2.3-2.5 on 1 February 2015. In Fig. 5 upper plot, level 2.0 AOD are marked. Level 2.0 data are usually used due to higher quality, and in this

particular case, have the same data-points as Level 1.5 data which are provided by the automatic cloud filtering algorithm of AERONET (Smirnov et al., 2000). As shown in Fig. 5, during the period of very high AOD values (before 12 UTC, AOD at 500 nm is higher than 1.9) the cloud screening procedure filtered out about 70% of data points (4 out of 13 passed this test). High AOD values in combination with rapid variation of them lead to the above result. Thus, for studying this dust case, we

5   will use the Level 1.05 AOD products and Level 1.5 inversions retrievals, keeping in mind the higher uncertainty that rises from this choice. The cloud-screened inversion data products derived from sky radiance measurements provided by the CIMEL were also used, and both the spectral single scattering albedo (SSA) and the aerosol volume size distribution, key aerosol properties for aerosol classification (see Taylor et al., 2015 and references therein) are presented in Fig. 5. The Level 1.5 SSA presents high values in the near-UV at 470nm that are in excess of 0.85 (rising to ≈0.97 in the visible) but

10   importantly, also have extremely low percentage sphericity (0.2-0.6%) as expected for aged dust grains (Dubovik et al., 2002). The typical signature of dust is also demonstrated by the Level 1.5 aerosol volume size distribution which shows a large peak centered on 3-4μm in line with expected microphysical properties of desert dust (Kinne et al., 2003; Taylor et al., 2014).

3.4 Impacts of dust on surface solar radiation

15   **3.4.1 RTM simulations**

The intensity of this dust case, was further investigated by comparinged the induced attenuation in SSR with the mean monthly attenuation percentages over Athens (ATHENS-NOA AERONET site). For this reason we calculated the mean monthly Level 1.5 AOD values and ranges based on an 8-years AERONET climatology (07/04/2008-31/03/2016) and the results are shown in Fig. 6. The range of climatological AODs is ≈ 0.11-0.22 with two peaks in Spring and Summer. Spring

20   is the most favourable season for dust transport from North Africa to Greece (e.g. Kalivitis et al. 2007; Kosmopoulos et al. 2008; Gerasopoulos et al. 2007; 2011), while the summer peak is related to transport of pollution from continental Europe (e.g. Gerasopoulos et al., 2011) and increased agricultural burning and forest fires (e.g. Athanasopoulou et al., 2014). The range of monthly minimum and maximum AOD values revealed two different peaks in Winter (2.36) and Autumn (1.63) something that indicates that the most extreme aerosol events occur in these two seasons. This finding has to do mainly with

25   intense dust transport in February (our dust case with AOD=1.21-2.36 and median value 1.71) and urban/industrial aerosols (Fameli et al., 2015; Kalivitis et al., 2007; Kosmopoulos et al., 2008), as well as wood burning cases with direct relations to the Greek economic crisis the last 7 years (Vrekoussis et al., 2013). These values were incorporated into the RTM and we simulated the GHI and DNI percentage attenuation at 40 and 60 degrees of solar zenith angle which are typical solar elevation angles for the region of Greece in the winter season. The results show significantly higher attenuation values for

30   larger SZAs and for DNI in general. In particular, at SZA of 40 degrees, the percentage decrease for GHI is around -5% and for DNI -17%, while at 60 degrees of SZA, the corresponding values are -7% and -25% respectively. All the above results are comparable with similar studies (Papadimas et al., 2012; Tumock et al., 2015; Qian et al., 2007), in terms of AOD range

(0.11-0.25 in EM) and mean aerosol radiative forcing under cloudless conditions (≈ -5% for GHI and -15% for DNI). Under the impact of the studied dust event as measured by AERONET, with median AOD in the specific site around 1.71, the GHI decrease is -37% at 40° and -49% at 60°, and the DNI is -80% and -90% at 40 and 60° respectively.

In Fig. 7 we simulated the radiative transfer (RT) using the AERONET station in Athens, in order to highlight the temporal variation of this dust case in 1-hour resolution, as well as the mean dust impact on the solar spectrum. In Fig. 7a we show the normalized spectral impact on the GHI for the region 285-1050 nm as spectral ratio of the irradiance under actual aerosol conditions to that under aerosol-free conditions. The higher spectral effect is found in the UVA region (around 400 nm) with attenuation of the order of 68%, while in the visible (400-700 nm) and the infrared regions the attenuation is almost 60% and 54%, respectively, indicating the weaker absorption of dust in these two spectral regions (Kaufman et al., 2000). These results are similar with relevant studies at various weather and atmospheric conditions (Dimberger et al., 2015; Ishii et al., 2013). In Fig. 7b the corresponding integrated ratios for GHI and DNI are shown. The stronger effect on DNI as compared to the GHI is apparent, which in Fig. 7b is depicted with DNI ratio values close to zero (absolute blocking) for the entire duration of the day.

In Fig. 8 the effect of dust is shown for various spectral integrals and quantities over Athens for the 1st of February 2015. These estimates were derived from RTM calculations based on actual aerosol conditions (AERONET data in Athens) and dust-free conditions. Specifically we show the diurnal course of DNI, GHI, UV-Index and irradiance in the Visible (VIS), together with the percentage attenuation for all occasions. Under dust-free conditions, the DNI ranges from 450 to 230 W/m^2, the GHI from 500 to 270 W/m^2, the VIS irradiance from 270 to 150 W/m^2 and the UV-Index from 2.6 to 0.8. Under the dust conditions, the highest values appeared in GHI (250-120 W/m^2) and the lowest in DNI (40-10 W/m^2) indicating the strong effect of dust on the direct component of SSR. These patterns are reflected in the percentage attenuation as well, with mean attenuation of -93% in DNI, followed by UV-Index (-70%), VIS (≈ -57%) and GHI (-53%) which is the minimum attenuation compared to all the other SSR fluxes.

Taking into account the significance of being able to forecasting the expected drastic reduction in SSR, as in the case of the particular dust plume, for e.g. CSP or PV installation management (PVs exploit the GHI and CSPs the DNI), in Fig. 9 we evaluated the CAMS' forecast at 12:00 UTC from both the total and dust AOD at 550nm found in the dataset described in Sect. 2.2.4, in terms of spatial and quantitative characteristics (Fig. 9). The dust AOD was found similar to the total AOD (dust AOD/total AOD >0.9 in the area), something that was depicted to the temporal (not shown) and spatial extent of the dust plume, demonstrating the effectiveness of CAMS and the fact that during dust outbreaks, the concentration of dust is tens of times greater than other aerosol species (Diaz et al., 2001). Figure 10 presents the RTM simulations using the CAMS AOD, as well as a direct comparison between the MODIS derived and simulated results with the CAMS 1 day-ahead forecasts. At Fig. 10a we present the MODIS level 3 and CAMS AODs at 550 nm in order to identify the observed (MODIS) and simulated/forecasted (CAMS) dust plume distribution, extent and AOD value intensity. The CAMS simulation follows the MODIS's observed dust plume extent, approaching its distribution but underestimating the peak AOD values (max MODIS values ≈ 3.5 and CAMS ≈ 1.9 over the Greek region). This underestimation pattern of the peak AOD valuesaerosol

~~direct radiative forcing~~, is a consequence of imperfect forecasted meteorology and fading impact of the initial assimilation of MODIS AOD info on CAMS performance (MACC, 2015; Allen et al., 2013). Yet, despite this difference, the impact on the energy and SSR simulations is of the order of 10% (see below description) in most cases (>90% of the spatial coverage), which highlights that CAMS 1-day ahead forecasts are really of great value and usefulness for solar energy potential

5   planning and policies (Langerock et al., 2015; Charabi and Gastli, 2015; Kosmopoulos et al., 2015; 2017; Ruiz-Arias et al., 2016). Since the main inputs to the RTM are the AOD and the SZA, which both can be forecasted (CAMS AOD) and pre-calculated (SZA), the real time spatial and temporal estimation of the dust events impact on SSR is realistically feasible. At Fig. 10b we simulated GHI (upper) and DNI (lower) under aerosol-free and under MODIS and CAMS aerosol conditions, near local-noon. In all cases we applied smoothing techniques in terms of data fitting to contour lines for better visualization

10   results. The SSR simulations were calculated with the impact of the dust as characterized in terms of high AOD values from MODIS level 3 values and CAMS 1-day ahead forecast. The retrieved AOD for the RTM calculations is at 550 nm, with spatial resolution of 1x1 and 0.4x0.4 degrees (MODIS and CAMS, respectively). The temporal resolution of MODIS overpass imaging is about 1 per day while for CAMS simulation is 1 per hour, highlighting also the ability of CAMS to provide significant information on the temporal evolution of solar energy availability. The panels in Fig. 10c describe the

15   impact on energy in terms of percentage attenuation of SSR indicating the radiative impact of the dust plume over Greece. The simulated results showed mean GHI values of about 500 W/m^2 for aerosol-free conditions, while for full aerosol conditions this value is reduced to about 300 W/m^2. The corresponding radiation values of DNI are 450 W/m^2 for clean and clear sky and around 80 W/m^2 for dust event conditions. We need to highlight as well that the maximum AOD that was simulated with the RTM was of the order of 3.5, which classifies this dust event as one of the most intense cases in the

20   eastern Mediterranean. In general, spring presents the higher frequency of dust events (Gerasopoulos et al., 2007; 2011; Gkikas et al., 2012; Kosmopoulos et al., 2008; 2017), while in winter occur the more intense dust events (Kalivitis et al., 2007). The percentage impact of the plume (Fig. 10c) is in the range 30-70% (MODIS) and 30-60% (CAMS) for the GHI and 70-100% and 60-90% (MODIS and CAMS, respectively) for DNI, highlighting and illustrating convincingly the extreme attenuation of the direct component of the total SSR and at the same time quantifying the energy exploitation losses

25   for PV and CSP applications. Overall, concerning the GHI and DNI percentage differences for the MODIS- and CAMS-based RTM simulation, we found that the CAMS forecasts overestimate the SSR values under high aerosol loads, indicating the limited ability of MACC to predict high AODs (MACC, 2015), while it can efficiently capture the dust plume extent and distribution. As a result, higher percentage differences on DNI following the highest AOD values and the lowest SSR values with minimum induced energy impact (DNI < 50 W/m^2) is found. The percentage differences for GHI reach 80-100% for

30   highest AOD values as well, with mean representative GHI attenuation below 50% (see Fig. 10c), highlighting the usefulness for energy forecasting needs and applications.

3.4.2 COSMO-ART simulations

Figure 11a depicts the event as captured by the COSMO-ART model application. In particular, the spatial distribution of the total AOD values (at 550nm, 12:00 UTC) is comparable with the respective satellite (MODIS) retrieval. Peak values are simulated over the Aegean Sea and they are higher (AOD = 5.2) compared to the satellite ones (AOD = 3.5). This is partly related to the higher spatial resolution of the model run (0.25°) in comparison to the satellite image (1°). Nevertheless, uncertainties in the dust source functions within aerosol models are common, and are usually treated by model tuning with respect to observations (e.g. Vogel et al., 2006; Miller et al., 2004), but this is outside the scope of the current study.

The implications of the interaction between the African dust plume and meteorology, are selectively shown in Fig. 11 (b and c plot). In particular, the incoming solar radiation in terms of GHI and DNI are examined, and their response to the dust plume during the daytime period (mean maximum AOD value ~ 3.5) is shown. As expected, the spatial pattern of the reduced solar energy that reaches the surface resembles that of the dust plume (Fig. 11a), because of the scattering and absorption of the incoming solar radiation by the dust particles. This decrease is more pronounced for the DNI, reaching values up to -180 Wm^{-2}, while the effect on the diffuse solar radiation is less intense (up to -100 Wm^{-2}, not shown). The effect on the GHI at the surface below the dust plume ranges between –200 Wm^{-2} (dust core) and –20 Wm^{-2} (dust edges), implying that the usage of solar energy in these areas (Cyclades and Crete) is greatly affected during the severe dust storm. This finding is comparable with values estimated in Rémy et. al. (2015), i.e. an effect of -300 Wm^{-2} at the heart of a dust storm over NE Africa (AOD ~ 3). The radiative effect of another dust storm over Western Europe (Bangert et al., 2012) was found smaller, as expected due to the low AOD values (up to 0.5). Considering the radiative efficiency (aerosol radiative effect per unit aerosol optical depth), our findings (60 Wm^{-2}) are smaller than those of Rémy et al. (2015) and Stanelle et al. (2010), but this is once more expected, as their findings correspond to hourly (noon) values (-140 to -150 Wm^{-2}), experienced over Africa.

Surprisingly, further inland in the Balkan peninsula, where the surface is less affected by the dust plume directly (AOD < 0.5, dust fraction < 0.4, Fig. 12a) increased amounts of DNI (Fig. 11c) are received, during the dust event. This is related to an increase of the air temperature within the plume (from surface to 2.5 km; not shown). This, in turn, creates a temperature gradient, which leads to a secondary atmospheric circulation towards the south. This is why the dust plume tongue is found shifted towards the south when the aerosol-meteorology interaction is switched on (base-case run) compared to the scenario with no interaction (not shown). Conclusively, the interaction of dust particles with the atmosphere leads to a positive feedback on solar radiation at the area north of the plume. These implications seem important, as the increase in the GHI (and DNI) is found +40 (+60) W m^{-2} over most of the positively-affected area. Similar dust radiative effects on the thermal gradient of the atmosphere have been already discussed in Stanelle et al. (2010).

This means that the interaction of dust particles with the atmosphere leads to a positive feedback on solar radiation at the area north of the plume. It is found that the plume tongue is shifted towards the south when the aerosol meteorology interaction is switched on (base case run) compared to the scenario with no interaction (not shown). This is related to an increase of the air temperature within the plume (from surface to 2.5 km; not shown), creating a temperature gradient, which leads to a secondary atmospheric circulation towards the south. The implications on the available solar energy seem

19

~~important, as the increase in the GHI (and DNI) is found +40 (+60) W m^{-2} over most of the positively-affected area. This follows the mechanism of thermal gradient creation due to the dust radiative effect discussed in Stanelle et al. (2010).~~

In order to further examine the spatial gradient of the dust effect on the short-wave radiation during the day, thus the hourly energy potential, the hourly zonal means are calculated and plotted (Fig. 12). The negative impact of the dust plume on the DNI, linked to great losses in solar energy potential for CSP systems, lasts from 06:00 to 15:00 UTC (February, 1) and maximizes at 11:00 UTC (-150 Wm^{-2}, average -80Wm^{-2} for the southern part of the domain). This value corresponds to more than 90% losses of DNI, due to the presence of the dust plume over south EM. The impact is limited for the rest of the area, ranging from -30 Wm^{-2} (maximum effect over the middle domain at 09:00 UTC) to +25 Wm^{-2} (maximum effect over the northern domain at 11:00 UTC). Nevertheless, percentage values are not negligible, reaching e.g. a dust impact on the DNI of +30% at the northern part of the domain and at 11:00 UTC. Similar is the dust impact on the GHI, referring though to greater absolute values (e.g. -400 Wm^{-2} from the base-case run over the southern domain at 10:00 and 11:00 UTC and -150Wm^{-2} from the scenario which does not take into account the interactions between dust particles and radiation). The consequent percentage losses of the solar energy potential for the PV systems reach 60% (maximum fraction, southern domain).

4. Summary and conclusions

This study reconfirms and quantifies high dust aerosol load impact on surface solar radiation, regional and local meteorology, modeling approaches and consequent horizontal and vertical structures and related phenomena. Understanding, determining the range of this impact on attenuation of the surface solar radiation, and providing timely and with adequate accuracy forecast, has major application to emerging solar energy exploitation application. We firstly mapped and studied the 3-D structure of a severe dust event occuring on 1 Feb 2015, via synergy of MODIS/Aqua and CALIOP/CALIPSO space-borne observations. The pure dust outflow yielded AOD$_{550nm}$ values higher than 3 in the plume center of mass, while extinction coefficient values were consistently larger than 0.2 km^{-1} and as high as 10 km^{-1}. Then RTM simulations were performed, using MODIS, CAMS and AERONET aerosol data as input. We found GHI values near local noon and under the dust plume of the order of 250 W/m^2 and 70 W/m^2, for DNI, while the simulated attenuation due to dust was on average -50% for GHI and -90% for DNI (below the dust plume), indicating the effective radiative influence of the dust particles during extreme dust cases. Under cloudless conditions aerosol plays a very important role. For example, the aerosol mean effect in Athens for AOD between 0.11 and 0.22 and for SZA 40° is 5% and 17% for GHI and DNI respectively, while in the presence of dust (i.e. 1 February 2015, AOD=1.71) the mean aerosol effect is increased, the order of 37% and 80% for GHI and DNI. At larger SZAs (e.g. 60°) this effect can reach values greater than 90%. CAMS provides AOD forecasts enabling forecasting solar energy and the aerosol impact. In this line, we highlighted the usefulness and accuracy (10% as compared with MODIS) of this aerosol forecast data stream, while using COSMO-ART we were able to quantify the important radiative impact of the dust plume over the EM (maximum daily value of the global radiative cooling over Crete is found

200 Wm^{-2}) and the respective mean energy losses for PV and CSP installations, which are consistent with the RTM simulations (≈40% and 80% for GHI and DNI respectively). Since satellite based observations and modeling results become more and easier accessible from year to year, their synergy is promising towards nowcasting, forecasting or analyzing past aerosol events, at spatial resolutions that surface based measurements cannot achieve. The synergistic use of satellite,

5 ground-based measurements and multi-faceted modeling techniques (RTM, CTM and CAMS) in this study, demonstrates the efficiency of such an approach in capturing the impact of dust storms (and expanding of this on other similar aerosol plumes) on SSR and of increasing our understanding of the Earth's radiation budget.

Nomenclature & abbreviations

AERONET	Aerosol Robotic Network
AF	Actinic Flux
AOD	Aerosol Optical Depth
ART	Aerosol and Reactive Trace gases
CAPIOL	Cloud Aerosol Lidar with Orthogonal Polarization
CALIPSO	Cloud-Aerosol Lidar and Infrared Pathfinder Satellite Observations
CAMS	Copernicus Atmosphere Monitoring Service
CF	Cloud Fraction
CSP	Concentrated Solar Plants
CTM	Chemical Transport Model
C6	Collection 6
DB	Deep Blue
DNI	Direct Normal Irradiance
DT	Dark Target
EARLINET	European Aerosol Lidar Network
ECMWF	European Centre for Medium-Range Weather Forecasts
EDGAR	Emission Database for Global Atmospheric Research
EM	Eastern Mediterranean
FNL	Final Analysis Data
GAW	Global Atmosphere Watch
GHI	Global Horizontal Irradiance
GOCART	Goddard Chemistry Aerosol Radiation and Transport
libRadtran	library for Radiative transfer
MACC	Monitoring Atmospheric Composition and Climate
MAPSS	Multi-sensor Aerosol Products Sampling System
MODIS	MODerate resolution Imaging Spectroradiometer

NCEP   National Centers for Environmental Protection
PV   Photovoltaics
RTM   Radiative Transfer Model
SSR   Surface Solar Radiation
SPEW   Speciated Particulate Emission Wizard
SSA   Single Scattering Albedo
SW   Shortwave
SZA   Solar Zenith Angle
TOA   Top of Atmosphere
UV   Ultraviolet
VIS   Visible

References

Allen, R. J., Norris, J. R., Wild, M.: Evaluation of multidecadal variability in CMIP5 surface solar radiation and inferred underestimation of aerosol direct effects over Europe, China, Japan, and India. Journal of Geophysical Research: Atmospheres, Volume 118 (12), 6311-6336. DOI: 10.1002/jgrd.50426., 2013.

5 Amiridis, V., Kafatos, M., Perez, C., Kazadzis, S., Gerasopoulos, E., Mamouri, R. E., ... and Zerefos, C.: The potential of the synergistic use of passive and active remote sensing measurements for the validation of a regional dust model. Ann. Geophys., 27, 3155-3164, 2009.

Amiridis, V., Marinou, E., Tsekeri, A., Wandinger, U., Schwarz, A., Giannakaki, E., ... and Ansmann, A.: LIVAS: a 3-D multi-wavelength aerosol/cloud database based on CALIPSO and EARLINET. Atmos. Chem. Phys., 15, 7127-7153,

10 doi:10.5194/acp-15-7127-2015, 2015.

Athanasopoulou, E., Rieger, D., Walter, C., Vogel., H., Karali, A., Hatzaki, M., ... and Roussos, A.: Fire risk, atmospheric chemistry and radiative forcing assessment of wildfires in eastern Mediterranean. Atmospheric Environment, 95, 113-125, 2014.

Athanasopoulou, E., Protonotariou, A., Papangelis, G., Tombrou, M., Mihalopoulos, N., and Gerasopoulos, E.: Long-range

15 transport of Saharan dust and chemical transformations over the Eastern Mediterranean. Atmospheric Environment, 140, 592-604, 2016.

Baldauf, M., Seifert, A., Förstner, J., Majewski, D., Raschendorfer, M. and Reinhardt, T.: Operational Convective-Scale Numerical Weather Prediction with the COSMO Model: Description and Sensitivities, Monthly Weather Review, 139(12), 3887–3905, doi:10.1175/MWR-D-10-05013.1, 2011.

20 Bangert, M., Kottmeier, C., Vogel, B. and Vogel, H.: Regional scale effects of the aerosol cloud interaction simulated with an online coupled comprehensive chemistry model, Atmospheric Chemistry and Physics, 11(9), 4411–4423, doi:10.5194/acp-11-4411-2011, 2011.

Bangert, M., Nenes, A., Vogel, B., Vogel, H., Barahona, D., Karydis, V. A., Kumar, P., Kottmeier, C. and Blahak, U.: Saharan dust event impacts on cloud formation and radiation over Western Europe, Atmospheric Chemistry and Physics,

25 12(9), 4045–4063, doi:10.5194/acp-12-4045-2012, 2012.

Benedetti, A., Morcrette, J. J., Boucher, O., Dethof, A., ... and the GEMS-AER team: Aerosol analysis and forecast in the ECMWF Integrated Forecast System. Part II : Data assimilation, Journal of Geophysical Research, 114, D13205, doi:10.1029/2008JD011115, 2009.

Boucher, O., Pham, M. and Venkataraman, C.: Simulation of the atmospheric sulfur cycle in the LMD GCM: Model description, model evaluation, and global and European budgets, Note 23, 26 pp., Inst. Pierre-Simon Laplace, Paris, France, 2002.

Cahalan, R., Oreopoulos, L., Marshak, A., Evans, F., Davis, A., ... & Zhuravleva, T.B.: The I3RC: Bringing Together the Most Advanced Radiative Transfer Tools for Cloudy Atmospheres. Bulletin of the American Meteorological Society, 86, 9, 1275-1293, 2005.

Charabi, Y. and Gastli, A. Spatio-temporal assessment of dust risk maps for solar energy systems using proxy data. Renewable Energy, 44, 23-31, 2012.

Claquin, T., Schulz, M., Balkanski, Y.m and Boucher, O.: Uncertainties in assessing radiative forcing by mineral dust. Tellus B 50, 491-505, 1998.

Dahlback, A., Stamnes, K. A.: new spherical model for computing the radiation field available for photolysis and heating at twilight. Planet Sp. Sci., 39, 671–83, 1991.

Dee, D.P., and Uppala, S.: Variational bias correction of satellite radiance data in the ERA-Interim reanalysis. Quarterly Journal of the royal meteorological society, 135, 1830-1841. DOI: 10.1002/qj.493, 2009.

Dentener, F., Kinne, S., Bond, T., Boucher, O., Cofala, J., Generoso, S., Ginoux, P., Gong, S., Hoelzemann, J.J., Ito, A. and Marelli, L.: Emissions of primary aerosol and precursor gases in the years 2000 and 1750 prescribed data-sets for AeroCom. Atmospheric Chemistry and Physics, 6(12), pp.4321-4344, 2006.

Diaz, J.P., Exposito, F.J., Torres, J., Herrera, F., Prospero, J.M., and Romero, M.C.: Radiative properties of aerosols in Saharan dust outbreaks using ground-based and satellite data: Applications to radiative forcing. J. Geophys. Res., 106, 18403-18416, 2001.

Dirnberger, D., Blackburn, G., Müller, B., & Reise, C.: On the impact of solar spectral irradiance on the yield of different PV technologies. Solar Energy Materials and Solar Cells, 132, 431-442, 2015.

Dubovik, O., Smirnov, A., Holben, B. N., King, M. D., Kaufman, Y. J., Eck, T. F., & Slutsker, I.: Accuracy assessments of aerosol optical properties retrieved from Aerosol Robotic Network (AERONET) Sun and sky radiance measurements. Journal of Geophysical Research: Atmospheres, 105(D8), 9791-9806, 2000.

Dubovik, O., Holben, B., Eck, T. F., Smirnov, A., Kaufman, Y. J., King, M. D., ... & Slutsker, I.: Variability of absorption and optical properties of key aerosol types observed in worldwide locations. Journal of the atmospheric sciences, 59(3), 590-608, 2002.

Emde, C., Buras-Schnell, R., Kylling, A., Mayer, B., Gasteiger, J., Hamann, U., ... & Bugliaro, L.: The libRadtran software package for radiative transfer calculations (version 2.0. 1). Geoscientific Model Development, 9(5), 1647-1672, 2016.

23

Emde, C., and Mayer, B.: Simulation of solar radiation during a total eclipse: a challenge for radiative transfer. Atmospheric Chemistry and Physics, 7, 2259-2270, 2007.

Flaounas, E., Kotroni, V., Lagouvardos, K., Kazadzis, S., Gkikas, A., & Hatzianastassiou, N.: Cyclone contribution to dust transport over the Mediterranean region. Atmospheric Science Letters, 16(4), 473-478, 2015.

5   Georgoulias, A. K., Alexandri, G., Kourtidis, K. A., Lelieveld, J., Zanis, P., Amiridis, V.: Differences between the MODIS Collection 6 and 5.1 aerosol datasets over the greater Mediterranean region. Atmos. Environ., 147, 310-319, doi:10.1016/j.atmosenv.2016.10.014, 2016.

Gerasopoulos, E., Koulouri, E., Kalivitis N., Kouvarakis, G., ... and Mihalopoulos N.: Size-segregated mass distributions of aerosols over Eastern Mediterranean: Seasonal variability and comparison with AERONET columnar size-distributions.
10   Atmos. Chem. Phys., 7, 2551-2561, 2007.

Gerasopoulos, E., Amiridis, V., Kazadzis, S., Kokkalis, P., Eleftheratos, K., Andreae, M. O., Andreae, T. W., El-Askary, H., Zerefos, C.S.: Three-year ground-based measurements of Aerosol Optical Depth over the Eastern Mediterranean: the urban environment of Athens. Atmos. Chem. Phys., 11, 2145-2159, doi:10.5194/acp-11-2145, 2011.

Gkikas, A., Houssos, E. E., Hatzianastassiou, N., Papadimas, C. D., and Bartzokas, A.: Synoptic conditions favouring the
15   occurrence of aerosol episodes over the broader Mediterranean basin. Quarterly Journal of the Royal Meteorological Society, 138(665), 932-949, 2012.

Gkikas, A., Hatzianastassiou, N., Mihalopoulos, N., Katsoulis, V., Kazadzis, S., Pey, J., ... and Torres, O.: The regime of desert dust episodes in the Mediterranean based on contemporary satellite observations and ground measurements. Atmos Chem Phys, 13, 12135-12154, 2013.

20   Gkikas, A., Basart, S., Hatzianastassiou, N., Marinou, E., Amiridis, V., Kazadzis, S., ... and Baldasano, J. M.: Mediterranean intense desert dust outbreaks and their vertical structure based on remote sensing data. Atmospheric Chemistry and Physics, 16, 8609-8642, 2016.

Grandey, B. S., Stier, P., & Wagner, T. M.: Investigating relationships between aerosol optical depth and cloud fraction using satellite, aerosol reanalysis and general circulation model data. Atmospheric Chemistry and Physics, 13(6), 3177-3184,
25   2013.

Guelle, W., Schulz, M., Balkanski, Y. and Dentener, F.: Influence of the source formulation on modeling the atmospheric global distribution of the sea salt aerosol, J. Geophys. Res., 106, 27,509– 27,524, 2001.

Haywood, J.M., Francis, P.N., Glew, M.D., and Taylor, J.P.: Optical properties and direct radiative effect of Saharan dust: A case study of two Saharan dust outbreaks using aircraft data. J. Geophys. Res., 106, 18417-18430, 2001.

30   Hess, M., Koepke, P., Schult, I.: Optical properties of aerosols and clouds: the software package OPAC. Bull. Am. Soc., 79, 831-844, 1998.

Holben, B. N., Eck, T. F., Slutsker, I., Tanre, D., Buis, J. P., Setzer, A., ... and Lavenu, F.: AERONET—A federated instrument network and data archive for aerosol characterization. Remote sensing of environment, 66(1), 1-16, 1998.

Holben, B. N., Tanre, D., Smirnov, A., Eck, T. F., Slutsker, I., Abuhassan, N., ... & Kaufman, Y. J.: An emerging ground-based aerosol climatology: Aerosol optical depth from AERONET. Journal of Geophysical Research: Atmospheres, 106(D11), 12067-12097, 2001.

Intergovernmental Panel on Climate Change (IPCC). Climate change 2013 The Physical Science Basis: Contribution of the

5   Working Group I to the Fifth Assessment Report of the IPCC. Cambridge University Press, New York, 2013.

Ishii, T., Otani, K., Takashima, T., and Xue, Y.: Solar spectral influence on the performance of photovoltaic (PV) modules under fine weather and cloudy weather conditions. Progress in Photovoltaics: Research and Applications, 21(4), 481-489, 2013.

Kalivitis, N., Gerasopoulos, E., Vrekoussis, M., Kouvarakis, G., Kubilay, N., Hatzianastassiou, N., Vardavas, I.,

10   Mihalopoulos, N.: Dust transport over the eastern Mediterranean derived from Total Ozone Mapping Spectrometer, Aerosol Robotic Network, and surface measurements. J. Geophys. Res., 112, D03202, doi:10.1029/2006JD007510, 2007.

Kato, S., Ackerman, T., Mather, J., Clothiaux, E.: The k-distribution method and correlated-k approxiamation for shortwave radiative transfer model. Journal of Quant Spectroscopy and Radiative Transfer, 62, 109-121, 1999.

Kaufman, Y.J., Karnieli, A., and Tanre, D.: Detection of dust over the desert by EOS-MODIS. IEEE Trans. Geosci. Remote

15   Sens., 38, 525-531, 2000.

Kaufman, Y.J., Tanre, D., Dubovic, O., Karnieli, A., ad Remer, L.A.: Absorption of sunlight by dust as inferred from satellite and ground-based remote sensing. Geophys. Res. Lett., 28, 1479-1482, 2001.

Kinne, S., and Pueschel, R.: Aerosol radiative forcing for Asian continental outflow. Atmospheric Environment 35, 5019-5028, 2001.

20   Kinne, S., Lohmann, U., Feichter, J., Schulz, M., Timmreck, C., Ghan, S., ... & Tegen, I.: Monthly averages of aerosol properties: A global comparison among models, satellite data, and AERONET ground data. Journal of Geophysical Research: Atmospheres, 108(D20), 2003.

Kosmopoulos, P. G., Kaskaoutis, D. G., Nastos P. T., and Kambezidis H. D.: Seasonal variation of columnar aerosol optical properties over Athens, Greece, based on MODIS data. Remote Sensing of Environment, 112, 2354-2366, 2008.

25   Kosmopoulos, P. G., Kaskaoutis, D. G., Prasad A. K., Sinha, P. R., and Rashki, A.R.: Spatial and vertical distribution of Sahara dust event over eastern Mediterranean in winter using remote sensing observations. 6th International Workshop on Sand/Duststorms and Associated Dustfall, Athens, Greece, 7-9 September, 2011.

Kosmopoulos, P. G., Kazadzis, S., Flocas, H. A., Marinou, E., Amiridis, V., Taylor, M., and Jacovidis, C.P.: A 3D aerosol climatology in the atmosphere of Greece by remote sensing and radiative transfer modeling techniques. Proceedings of the

30   12th International Conference on Meteorology, Climatology & Atmospheric Physics, Vol 2, 13-17, ISBN: 978-960-524-430-9, 2014.

Kosmopoulos, P. G., Kazadzis, S., Lagouvardos, K., Kotroni, V., and Bais A.: Solar Energy prediction and verification using operational model forecasts and ground-based solar measurements. Energy, 93, 1918-1930, 2015.

Kosmopoulos, P. G., Kazadzis, S., Taylor, M., Bais, A., Lagouvardos, K., Kotroni, V., Keramitsoglou, I., Kiranoudis, C.: Estimation of the solar energy potential in Greece using satellite and ground-based observations. Perspectives on Atmospheric Sciences, 1149-1156, 2017.

Kuenen, J. J. P., Visschedijk, A. J. H., Jozwicka, M. and Denier van der Gon, H. A. C.: TNO-MACC_II emission inventory; a multi-year (2003–2009) consistent high-resolution European emission inventory for air quality modelling, Atmos. Chem. Phys., 14(20), 10963–10976, doi:10.5194/acp-14-10963-2014, 2014.

Langerock, B., Mazière, M. D., Hendrick, F., Vigouroux, C., Desmet, F., Dils, B., & Niemeijer, S.: Description of algorithms for co-locating and comparing gridded model data with remote-sensing observations. Geoscientific Model Development, 8(3), 911-921, 2015.

Levy, R. C., Mattoo, S., Munchak, L. A., Remer, L. A., Sayer, A. M., Patadia, F., & Hsu, N. C.: The Collection 6 MODIS aerosol products over land and ocean. Atmos. Meas. Tech, 6(11), 2989-3034, 2013.

Li, F., Vogelmann, A.M., and Ramanathan, V.: Saharan dust aerosol radiative forcing measured from space. Journal of Climate, 17, 2558-2571, 2004.

Lindfors, A. V., Kouremeti, N., Arola, A., Kazadzis, S., Bais, A. F., and Laaksonen, A.: Effective aerosol optical depth from pyranometer measurements of surface solar radiation (global radiation) at Thessaloniki, Greece. Atmospheric Chemistry and Physics, 13(7), 3733-3741, 2013.

MACC near-real time global atmospheric composition service (Validation report): System evolution and performance statistics (Status up to 1 March 2015). MACC-III Deliverable D37.6, 2015, File: MACCIII_VAL_DEL_D_37.6_ NRTReport04_20150528, 2015.

Mamouri, R. E., Ansmann, A., Nisantzi, A., Solomos, S., Kallos, G., & Hadjimitsis, D. G.: Extreme dust storm over the eastern Mediterranean in September 2015: satellite, lidar, and surface observations in the Cyprus region. Atmospheric Chemistry and Physics, 16(21), 13711-13724, 2016.

Marquart, S., and Mayer, B.: Towards a reliable GCM estimation of contrail radiative forcing. Geophys. Res. Lett., 29, 8, 1179, 2002.

Mayer, B., and Kylling, A.: Technical note: The libRadtran software package for radiative transfer calculations - description and examples of use. Atmos Chem Phys 5, 1855-1877, 2005.

Miller, R.L., Tegen, I., and Perlwitz J.: Surface radiative forcing by soil dust aerosols and the hydrologic cycle. J. Geophys. Res., 109, D04203, doi:10.1029/2003JD004085, 2004.

Morcrette, J.-J., Beljaars, A., Benedetti, A., Jones, L., and Boucher, O.: Sea-salt and dust aerosols in the ECMWF IFS model , Geophys. Res. Lett., 35, L24813, doi:10.1029/2008GL036041, 2008.

Morcrette, J.-J., Boucher, O., Jones, L., Salmond, D., Bechtold, P., ... and Untch, A.: Aerosol analysis and forecast in the ECMWF Integrated Forecast System. Part I: Forward modelling, Journal of Geophysical Research, 114D, D06206, doi:10.1029/2008JD011235, 2009.

NCEP/National Weather Service/NOAA/U.S. Department of Commerce. 2000, updated daily. NCEP FNL Operational Model Global Tropospheric Analyses, continuing from July 1999. Research Data Archive at the National Center for Atmospheric Research, Computational and Information Systems Laboratory. https://doi.org/10.5065/D6M043C6, 2000.

Nyamsi, W., Espinar, B., Blanc, P., Wald, L.: How close to detailed spectral calculations is the k-distribution method and correlated-k approximation of Kato et al. (1999) in each spectral interval? Meteorologische Zeitschrift Vol. 23 No. 5, p. 547-556, 2014.

Omar, A., Winker, D., Kittaka, C., Vaughan, M., Liu, Z., Hu, Y. X., Trepte, C., Rogers, R., Ferrare, R., Lee, K., Kuehn, R., and Hostetler, C.: The CALIPSO automated aerosol classification and lidar ratio selection algorithm, J. Atmos. Ocean. Tech., 26, 1994–2014, doi:10.1175/2009jtecha1231.1, 2009.

Omar, A., Tackett, J., Magill, B. Vaughan, M., Kar, J., Winker D., and Trepte, C.: Enhancements to the CALIOP aerosol subtyping and lidar ratio selection algorithms for Level II version 4, CALIPSO/CloudSat 2016 Science Team Meeting, Newport News, Virginia, 1-3 March 2016 (link: https://www-calipso.larc.nasa.gov/resources/calipso_users_guide/ qs/qs_lid_l2_all_v4-10_files/2OmarSubtypingPoster. pdf), 2016.

Pandithurai, G., Dipu, S., Dani, K.K., Tiwari, S., ... and Pinker R.T.: Aerosol radiative forcing during dust events over New Delhi, India. J. Geophys. Res., 113, D13209, 2008.

Papadimas, C.D., Hatzianastassiou, N., Matsoukas, C., Kanakidou, M., Mihalopoulos, N. and Vardavas, I.: The direct effect of aerosols on solar radiation over the broader Mediterranean basin. Atmospheric Chemistry and Physics, 12(15):7165-7185, 2012.

Papayannis, A., Balis, D., Amiridis, V., Chourdakis, G., Tsaknakis, G., Zerefos, C., ... and Grabowski, J.: Measurements of Saharan dust aerosols over the Eastern Mediterranean using elastic backscatter-Raman lidar, spectrophotometric and satellite observations in the frame of the EARLINET project. Atmospheric Chemistry and Physics, 5(8), 2065-2079, 2005.

Petrenko, M., Ichoku, C., and Leptoukh, G.: Multi-sensor Aerosol Products Sampling System (MAPSS), Atmos. Meas. Tech., 5, 913-926, doi:10.5194/amt-5-913-2012, 2012.

Platnick, S., Meyer, K. G., King, M. D., Wind, G., Amarasinghe, N., Marchant, B., ... and Yang, P.: The MODIS Cloud Optical and Microphysical Products: Collection 6 Updates and Examples From Terra and Aqua. IEEE Transactions on Geoscience and Remote Sensing, 2016.

Qian, Y., Wang, W., Leung, L. R., and Kaiser, D. P.: Variability of solar radiation under cloud-free skies in China: The role of aerosols. Geophysical Research Letters, 34(12), 2007.

Reddy, M. S., Boucher, O., Bellouin, N., Schulz, M., Balkanski, Y., Dufresne, J.-L., and Pham, M.: Estimates of global multi-component aerosol optical depth and direct radiative perturbation in the Laboratoire de Météorologie Dynamique general circulation model, Journal of Geophysical Research, 110, D10S16, doi:10.1029/2004JD004757, 2005.

Rémy, S., Benedetti, A., Bozzo, A., Haiden, T., Jones, L., Razinger, M., Flemming, J., Engelen, R. J., Peuch, V. H. and Thepaut, J. N.: Feedbacks of dust and boundary layer meteorology during a dust storm in the eastern Mediterranean, Atmospheric Chemistry and Physics, 15(22), 12909–12933, doi:10.5194/acp-15-12909-2015, 2015.

Rieger, D., Bangert, M., Kottmeier, C., Vogel, H. and Vogel, B.: Impact of aerosol on post-frontal convective clouds over Germany, Tellus B: Chemical and Physical Meteorology, 66(1), 22528, doi:10.3402/tellusb.v66.22528, 2014.

Rockel, B., Will, A. and Hense, A.: The Regional Climate Model COSMO-CLM (CCLM), Meteorologische Zeitschrift, 347–348, doi:10.1127/0941-2948/2008/0309, 2008.

5 Ruiz-Arias, J. A., Gueymard, C. A., Santos-Alamillos, F. J., Poza-Vazquez, D.: Worldwide impact of aerosol's time scale on the predicted long[term concentrating solar power potential. Nature, Scientific Reports, 6:30546, DOI:10.1038/srep30546, 2016.

Salomonson, V.V., Barnes, W.L., Maymon, P.W., Montgomery, H.E., Ostrow, H.: MODIS: advanced facility instrument for studies of the Earth as a system. IEEE Trans. Geosci. Remote 27, 145e153, 1989.

10 Sayer, A. M., Hsu, N. C., Bettenhausen, C., Jeong, M., Meister, G., Al, S.E.T.: Effect of MODIS Terra radiometric calibration improvements on Collection 6 deep Blue aerosol products: validation and Terra/Aqua consistency. J. Geophys. Res. Atmos. 120 (23), 12157e12174. http://dx.doi.org/10.1002/2015JD023878, 2015.

Schulz, M., de Leeuw, G., and Balkanski, Y.: Sea-salt aerosol source functions and emissions, in Emission of Atmospheric Trace Compounds, edited by C. Granier, P. Artaxo, and C. E. Reeves, pp. 333–354, Kluwer Acad., Norwell, Mass, 2004.

15 Schwartz, S. E., Charlson, R. J., Kahn, R., Rodhe, H.: Earth's climate sensitivity: apparent in consistencies in recent assessments. Earth's Future, 2, 601–5, 2014.

Shettl,e E. P.: Models of aerosols, clouds and precipitation for atmospheric propagation studies. In: Proceedings of AGARD conference 454 on atmospheric propagation in the UV, visible, IR and MM-region and related system aspects, 1989.

Smirnov, A., Holben, B. N., Eck, T. F., Dubovik, O., Slutsker, I.: Cloud screening and quality control algorithms for the
20 AERONET data base. Remote Sensing of Environment 73, 337-349, 2000.

Stanelle, T., Vogel, B., Vogel, H., Bäumer, D. and Kottmeier, C.: Feedback between dust particles and atmospheric processes over West Africa during dust episodes in March 2006 and June 2007, Atmospheric Chemistry and Physics, 10(22), 10771–10788, doi:10.5194/acp-10-10771-2010, 2010.

Stein, A.F., Draxler R.R., Rolph G.D., Stunder B.J.B., Cohen M.D., Ngan F.: NOAA's HYSPLIT atmospheric transport and
25 dispersion modeling system. Bull. Amer. Meteor. Soc. 96(12), 2059-2077, 2015.

Taylor, M., Kazadzis, S., Gerosopoulos, E.: Multi-modal analysis of aerosol robotic network size distributions for remote sensing applications: dominant aerosol type cases. Atmospheric Measurement Techniques, 7(3), 839-858, dx.doi.org/ 10.5194/amt-7-839-2014, 2014.

Taylor, M., Kazadzis, S., Amiridis, V., Kahn, R.A.: Global aerosol mixtures and their multiyear and seasonal characteristics.
30 Atmospheric Environment, 116, 112-129, dx.doi.org/10.1016/j.atmosenv.2015.06.029, 2015.

Tegen, I., Lacis, A.A., Fung, I.: The influence of climate forcing of mineral aerosols from disturbed soils. Nature, Apr. 4, 380, 6573, ProQuest pg. 419, 1996.

Tesche, M., Ansmann, A., Müller, D., Althausen, D., Engelmann, R., Freudenthaler, V., and Groß, S.: Vertically resolved separation of dust and smoke over Cape Verde using multiwavelength Raman and polarization lidars during Saharan Mineral Dust Experiment 2008, J. Geophys. Res.-Atmos., 114, D13202, doi: 10.1029/2009JD011862, 2009.

5   Turnock, S.T., Spracklen, D.V., Carslaw, K.S., Mann, G.W., Woodhouse, M.T., Forster, P.M., Haywood, J., Johnson, C.E., Dalvi, M., Bellouin, N., and Sánchez-Lorenzo, A.: Modelled and observed changes in aerosols and surface solar radiation over Europe between 1960 and 2009. Atmospheric Chemistry and Physics, 15(16):9477-9500, 2015.

Vaughan, M.A., Powell, K.A., Kuehn, R.E., Young, S.A., Winker, D.M., ... and Getzewich, B.J.: Fully automated detection of cloud and aerosol layers in the CALIPSO lidar measurements. Journal of Atmosph. and Oceanic Technol., 26 (10), 2034-2050, 2009.

10   Vogel, B., Vogel, H., Bäumer, D., Bangert, M., Lundgren, K., Rinke, R., and Stanelle, T.: The comprehensive model system COSMO-ART–Radiative impact of aerosol on the state of the atmosphere on the regional scale. Atmospheric Chemistry and Physics, 9(22), 8661-8680, 2009.

Vogel, B., Hoose, C., Vogel, H., Kottmeier, C.; A model of dust transport applied to the Dead Sea Area. Meteorol. Z. 15, 611–624, 2006.

15   Vrekoussis, M., Richter, A., Hilboll, A., Burrows, J. P., ... and Mihalopoulos N.: Economic crisis detected from space: Air quality observations over Athens/Greece. Geoph. Res. Letters, 40, 1-6, doi:10.1002/grl.50118, 2013.

Winker, D. M., Vaughan, M. A., Omar, A. H., Hu, Y., Powell, K. A., Liu, Z., Hunt, W. H., and Young, S. A.: Overview of the CALIPSO Mission and CALIOP Data Processing Algorithms, J. Atmos. Oceanic Technol., vol 26, pp. 2310–2323, doi: 10.1175/2009JTECHA1281.1, 2009.

20   Zängl, G., Reinert, D., Rípodas, P., and Baldauf, M.: The ICON (ICOsahedral Non-hydrostatic) modelling framework of DWD and MPI-M: Description of the non-hydrostatic dynamical core, Quarterly Journal of the Royal Meteorological Society, 141(687), 563–579, doi:10.1002/qj.2378, 2015.

25

30

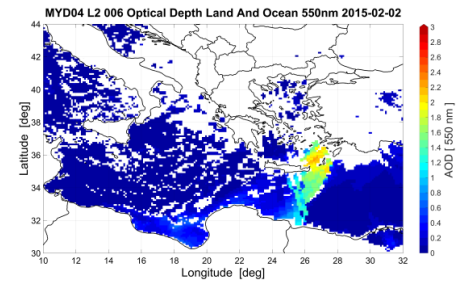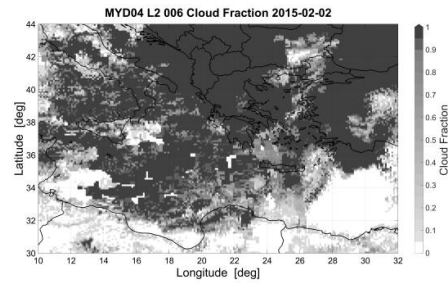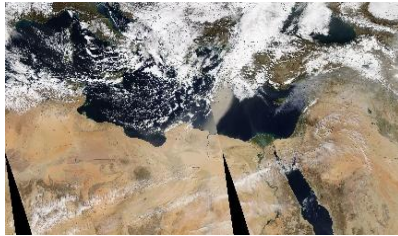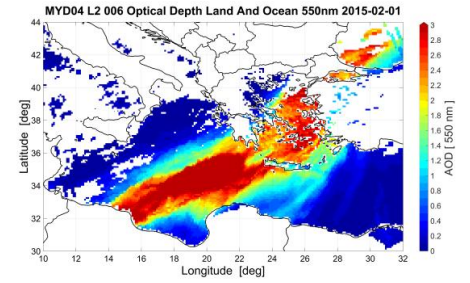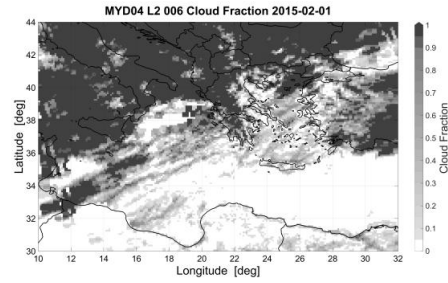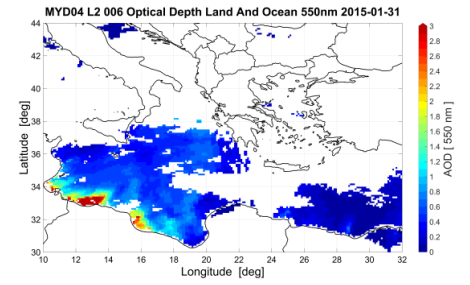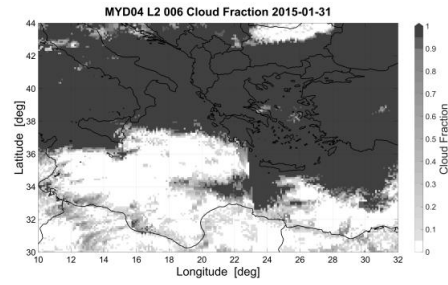(a)   (b)
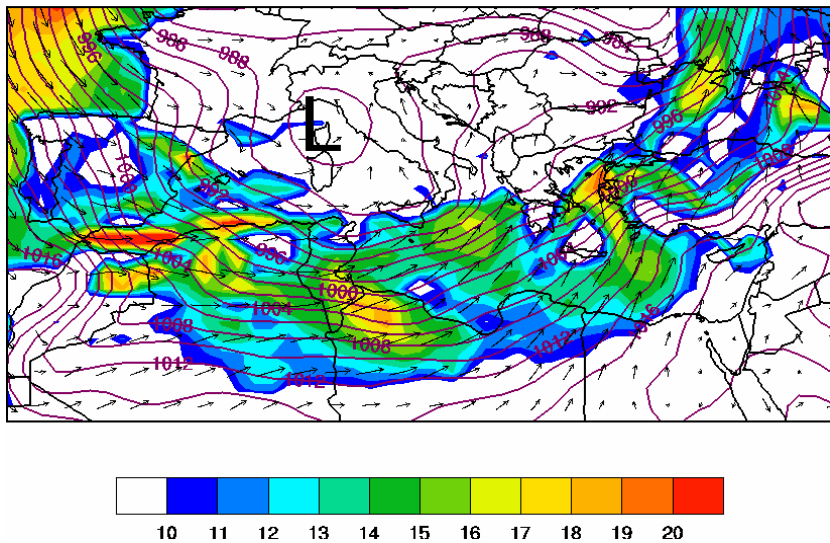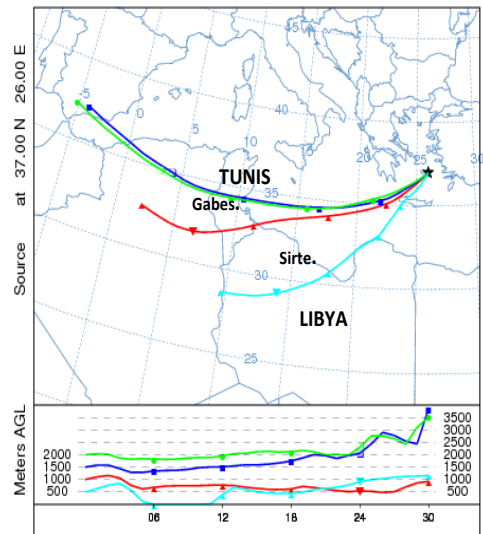
Figure 1: NCEP final analysis data (FNL) at 12:00 UTC, 31 January 2015 (a). The wind speed > 10 ms⁻¹ at 1000 hPa is shown (color scale and vectors) overlaid with mean sea level pressure (contour lines). The low pressure center is denoted with L. The HYSPLIT back-trajectories arriving over the Aegean Sea at 12:00 UTC, 1 February 2015 (b).

5

10

15

20

25

(a)   **(b)**   **(c)**

Figure 2: Satellite observation of the temporal evolution of the dust incursion peaking on 1 Feb 2015 over Greece from MODIS/Aqua satellite data. (a) True colour imagery based on Bands 1,3 and 4. (b) Evolution of the cloud fraction and (c) AOD on the day before (top), during (centre) and after (bottom) peak dust. Note that the days either side of the peak are extensively cloud covered. High values of AOD were observed up to 3 days prior and after the peak.
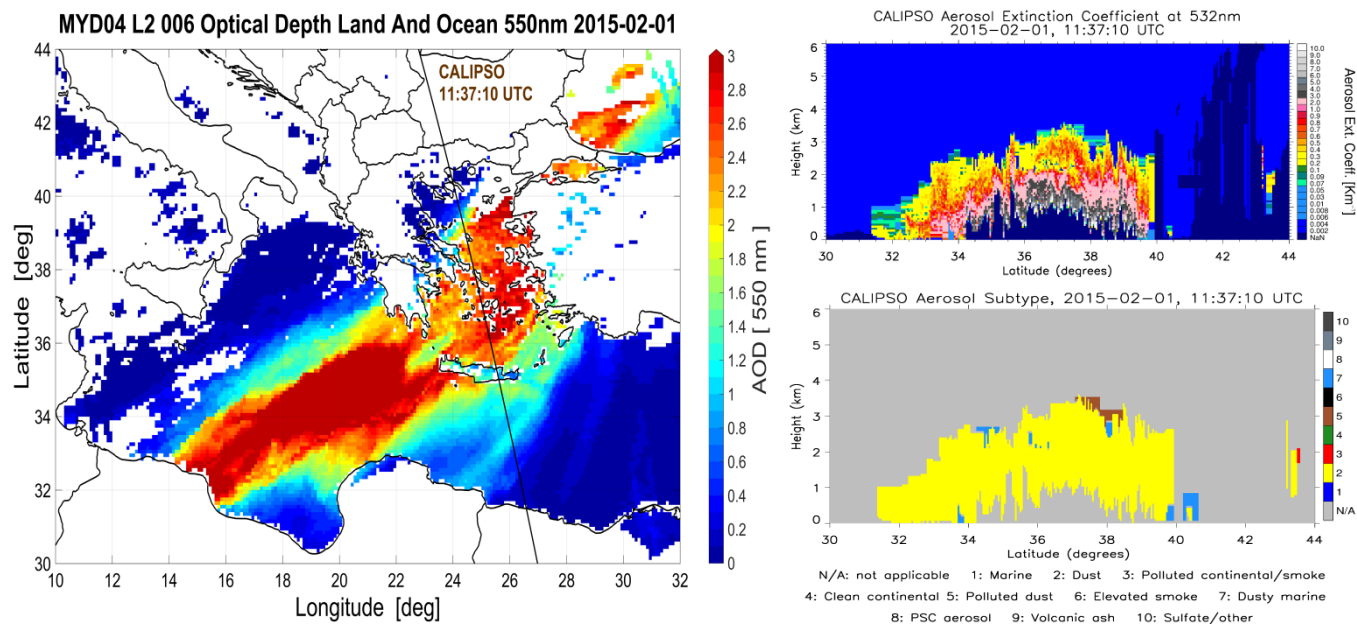
Figure 3: 3D profiling of the dust incursion on 1 Feb 2015: spatial extent provided by MODIS Level 2 (collection 6) AOD at 550nm (Left) together with CALIPSO profiles at 532nm of the extinction coefficient (Upper Right) and aerosol sub-typing (Lower Right) in the profile taken at 11:37 UTC (indicated by the distinct black-coloured track line in the left panel).

5

Land AOD-mean(Complete), '06-'10, seasons: All, QA: pre-filtered, at All_Locations, outliers removed

AMODIS: R²=0.80,RMSE=0.09, y=0.95x+0.01, N=47483, outliers=1371

(a)

Land AOD-mean(Complete), '06-'10, seasons: All, QA: pre-filtered, at ATHENS-NOA, outliers removed

AMODIS: R²=0.63,RMSE=0.08, y=0.93x+0.05, N=156, outliers=0

(b)
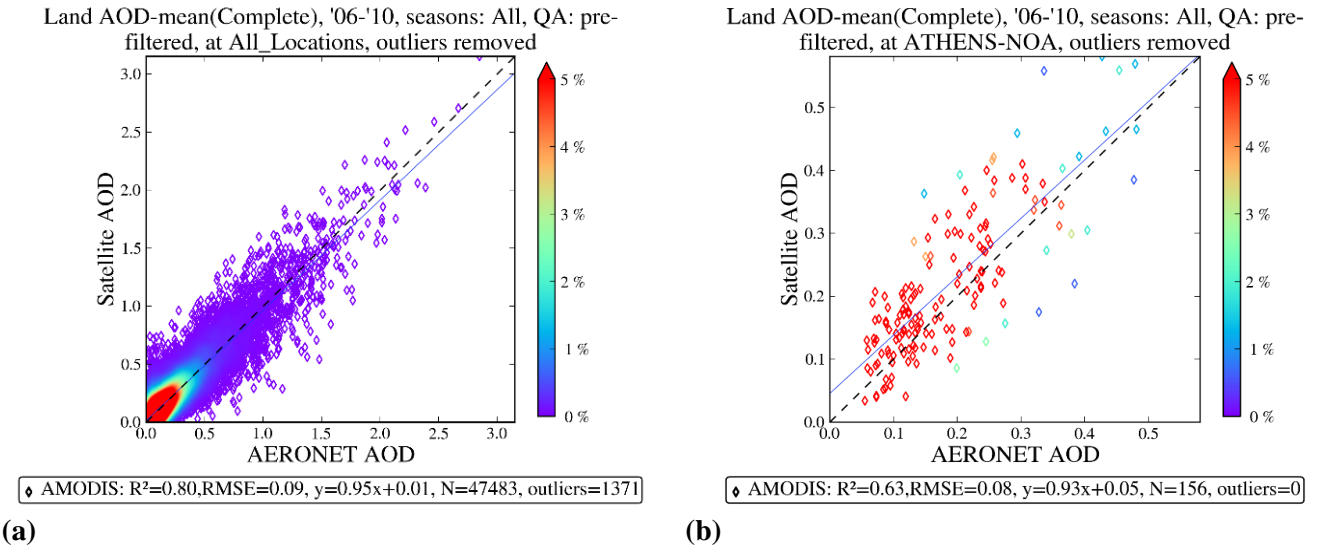
10 **Figure 4: Scatter plots of satellite AOD (550nm) from MODIS/Aqua versus coincident AOD from AERONET for the five year period 2006-2010 with outliers removed. (a) shows the global record and (b) is for the ATHENS-NOA site. The colour bar describes the percentage frequency of AOD values occurrence (source of the plots: https://giovanni.gsfc.nasa.gov/mapss_explorer).**

15

20

25

30

35
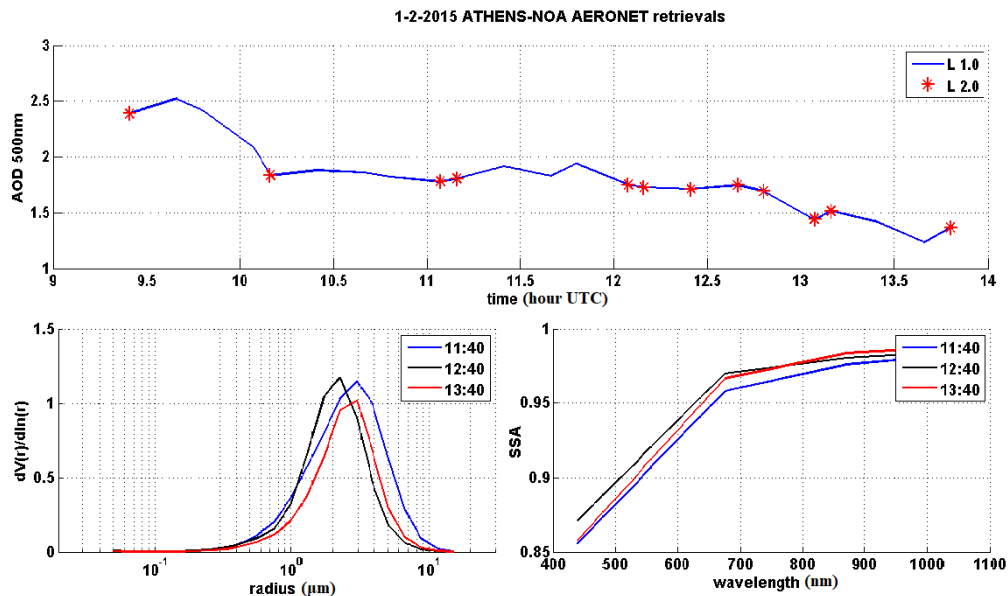
Figure 5: Temporal evolution of the AOD at 500 nm obtained from the Level 1.0 and 2.0 inversion algorithm of the CIMEL sunphotometer at the Athens site during the day of peak dust incursion over the region on 1 Feb 2015 (upper) together with aerosol volume size distribution (lower left) and the spectral SSA (lower right) retrieved from the Level 1.5 inversion algorithm on the same day.
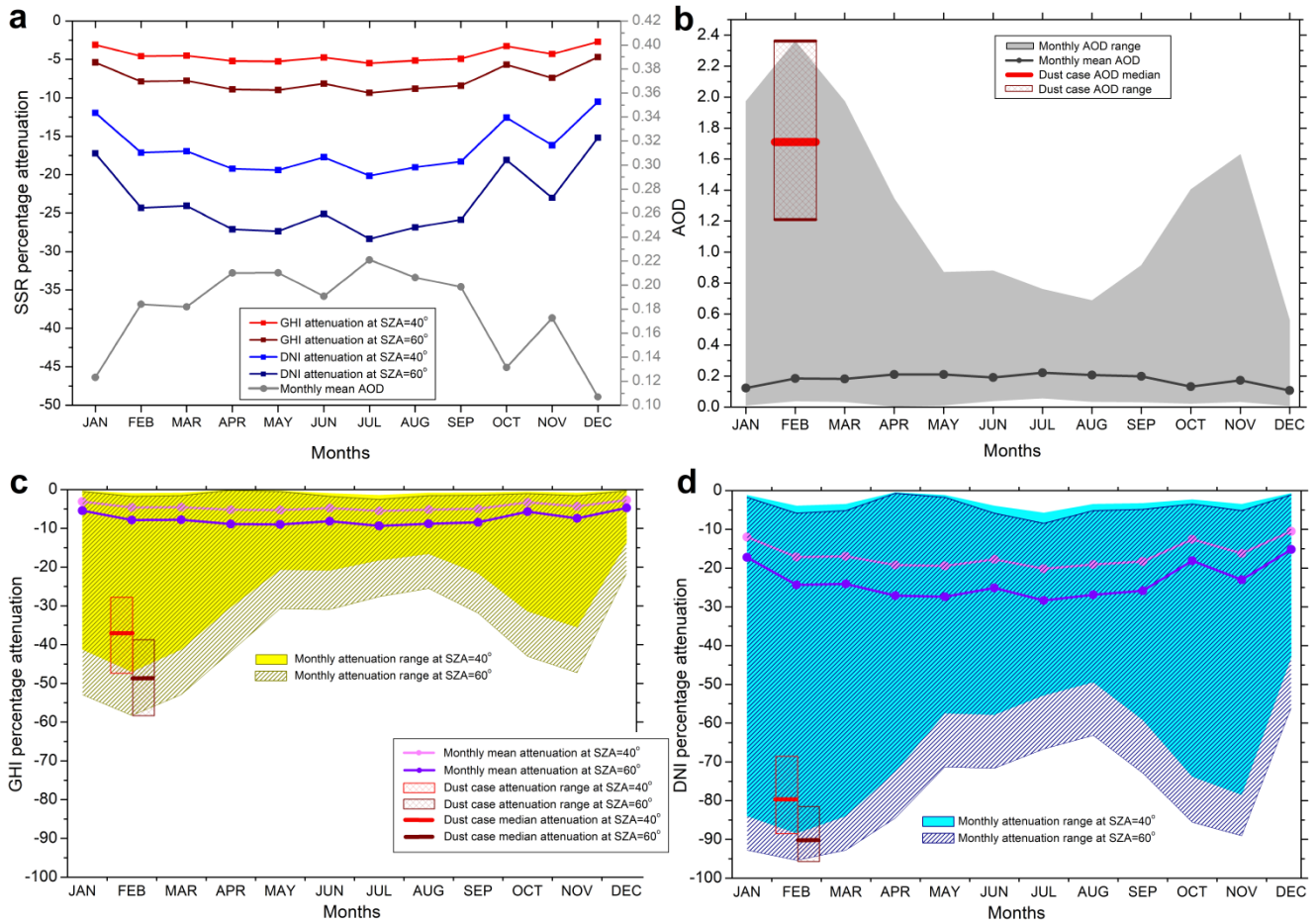
Figure 6: Mean monthly GHI and DNI percentage attenuation in Athens as a function of solar zenith angle and AOD (a) together with the mean monthly range of AOD (b), the percentage attenuation range for GHI (c) and DNI (d). The red-shaded insets shows the corresponding median values and ranges at the peak of the strong dust incursion over the region on 1 Feb 2015.
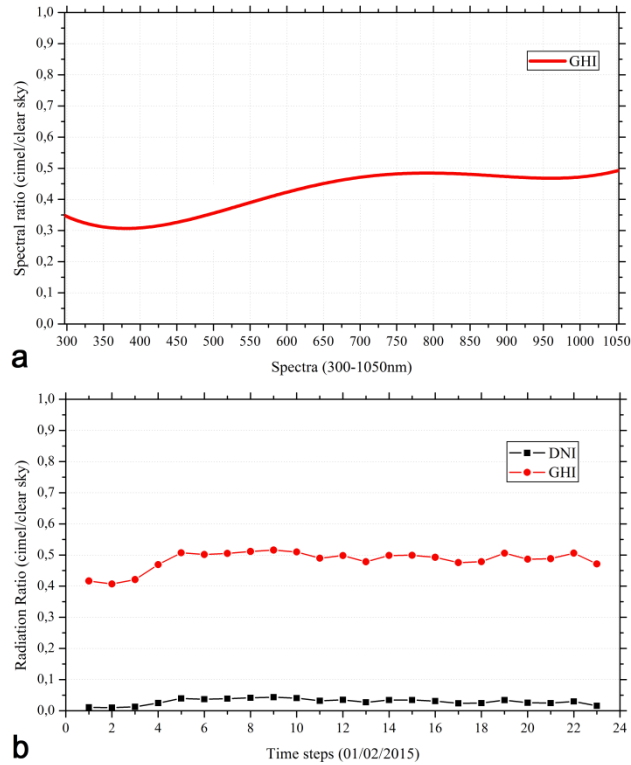
Figure 7: (a) The spectral effect of the extreme dust event of 1 Feb 2015 at the Athens station as depicted by the ratio of the AERONET Cimel sunphotometer irradiance to the clear sky irradiance calculated with a RTM for the same atmospheric conditions. Note the increased attenuation at shorter wavelengths. (b) Temporal evolution of the hourly value of the ratio for the GHI and DNI output by the RTM.
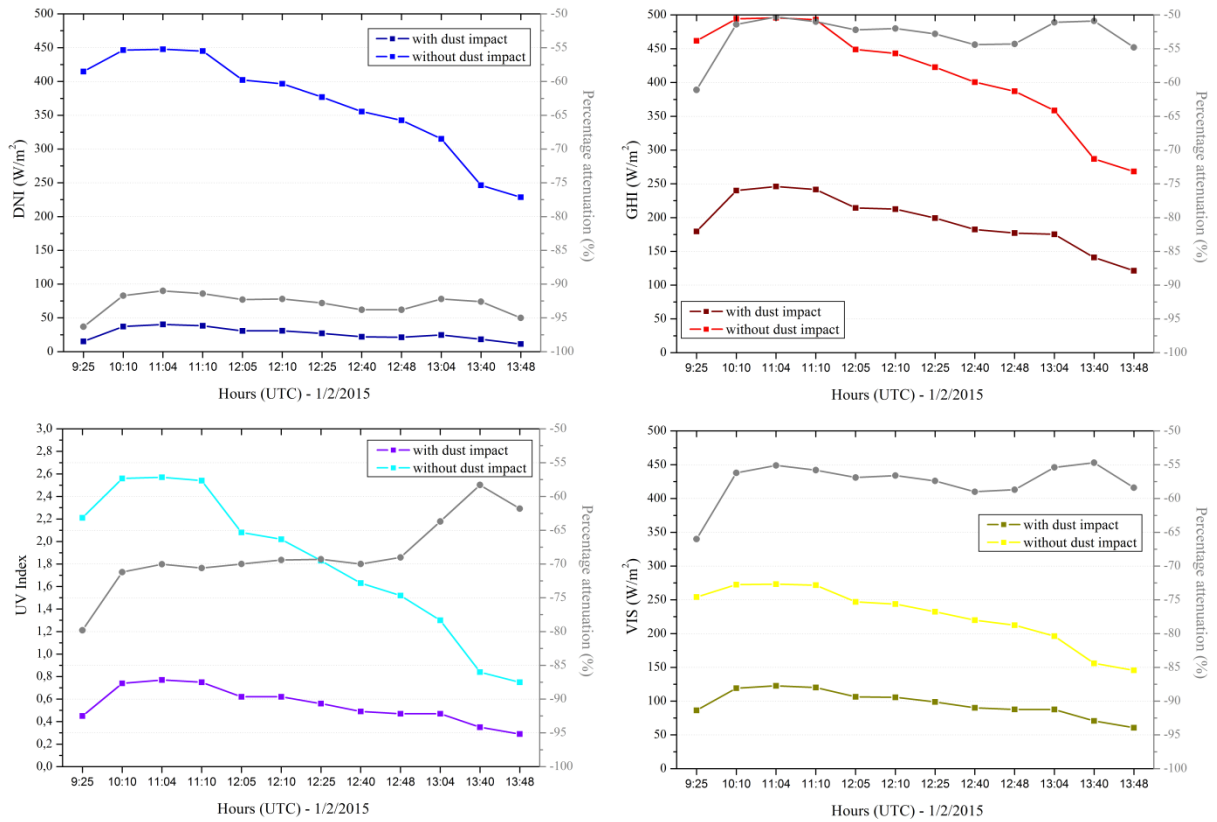
5 | **Figure 8: Temporal evolution of GHI, DNI, UV Index and VIS irradiances during the extreme dust event of 1 Feb 2015 at the Athens station. The modeled values (without dust impact) coincident with AERONET Cimel measurements (with dust impact) are shown together with the % attenuation due to impact of dust.**
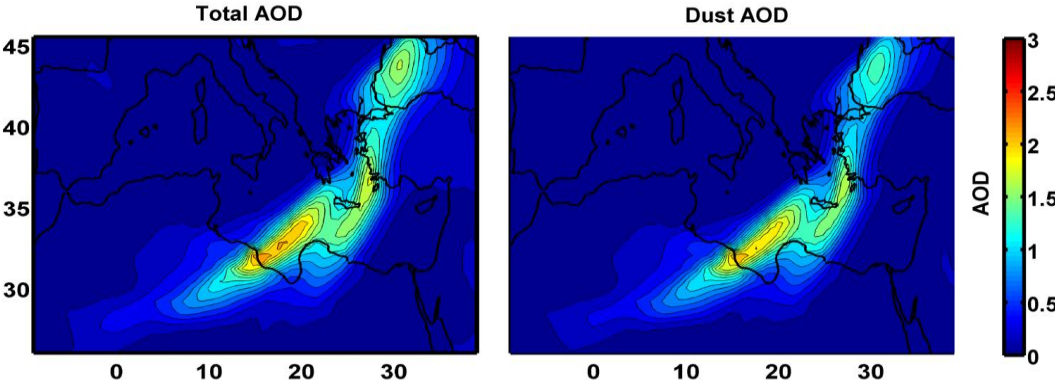
10

15

20

25

Figure 9: The spatial extent of total AOD (left) and dust AOD (right) at 550nm provided by CAMS. These maps depict predictions by the MACC one-day-ahead forecast (spatial resolution: 0.4 x 0.4 degrees). The maps correspond to 12:00 UTC, when maximum AOD ≈ 2.3. The temporal resolution of the forecast is 1 hour.
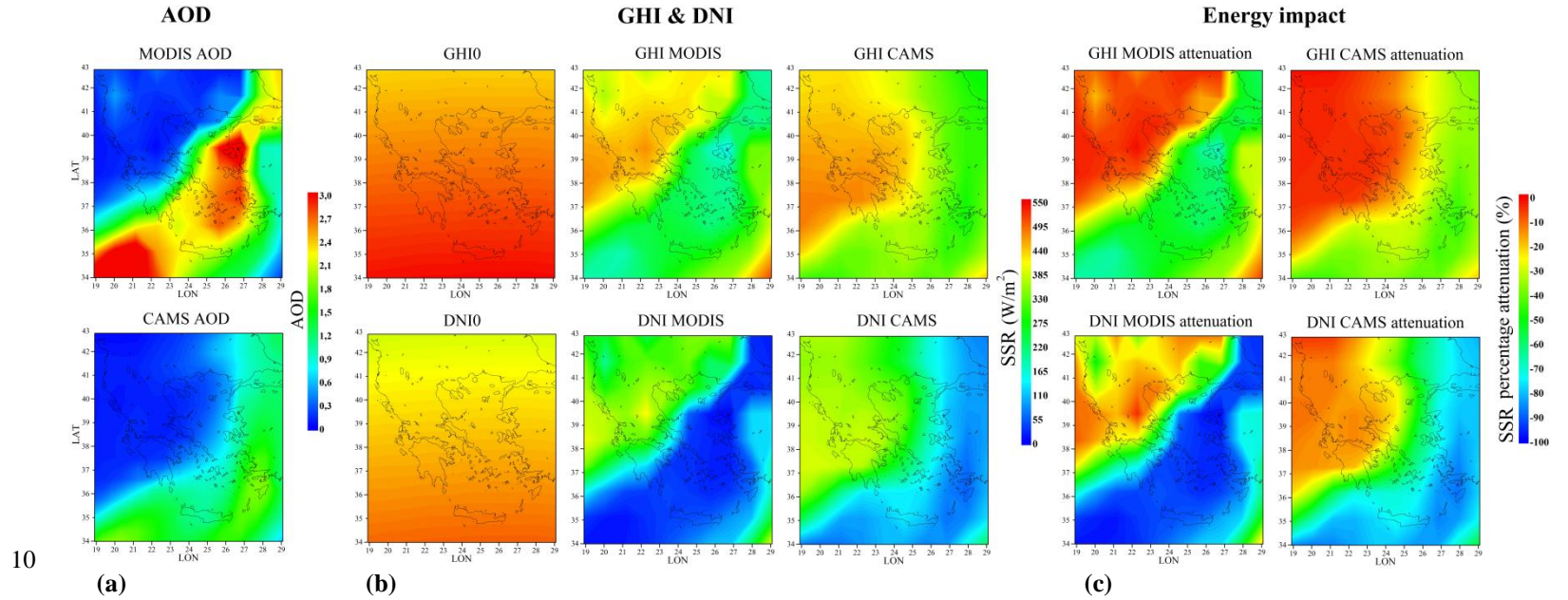
15

20

25

30

Figure 10: (a) AOD from MODIS level 3 and the CAMS 1-day ahead forecast. (b) RTM simulations at local noon on the day of the incursion on 1 Feb 2015 for GHI and DNI. GHI0 and DNI0 represent the simulations without dust (with only the effects of SZA). (c) The energy impact in terms of percentage attenuation relative to the dust-free simulations for GHI and DNI under MODIS- and CAMS-based AODs. For the GHI, the attenuation is about 30 – 70 % for MODIS and about 30 - 60 % for CAMS. For the DNI, the attenuation is about 70 – 100 % for MODIS and about 60 - 90 % for CAMS.

(a) (b) (c)
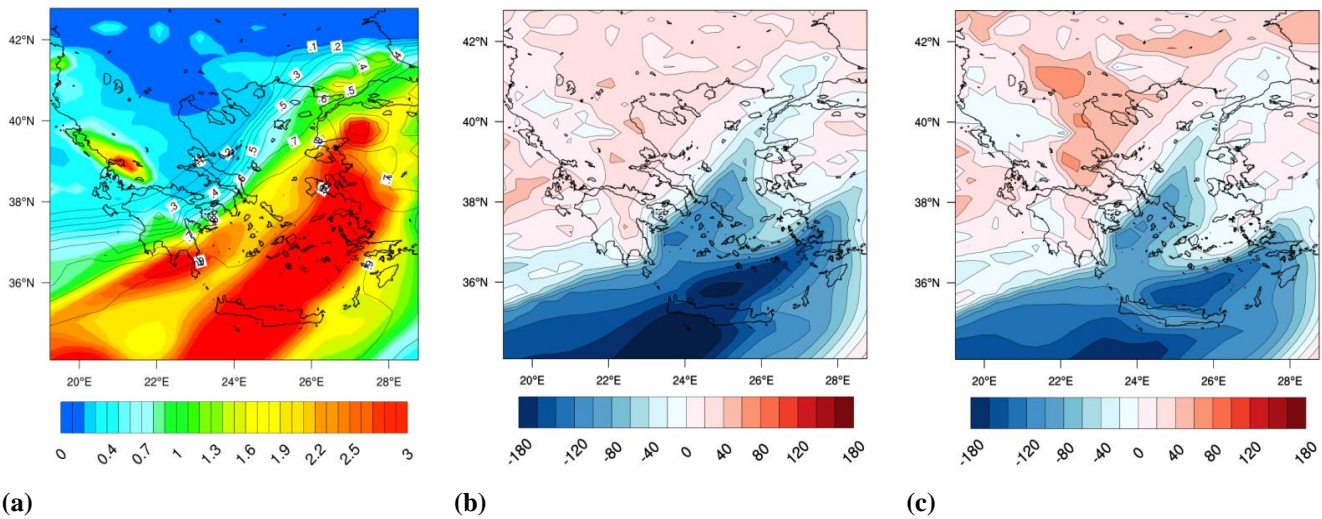
Figure 11: The spatial distribution of the: (a) total AOD (at 550nm). Iso-lines indicate the dust fraction of the total AOD model values. The map corresponds to 12:00 UTC, when maximum AOD ≈ 5.2. (b) dust plume effect on GHI and (c) DNI (in W/m^2) at surface, averaged for the daytime hours of the extreme dust event of 1 Feb 2015 over Greece as predicted by COSMO-ART.
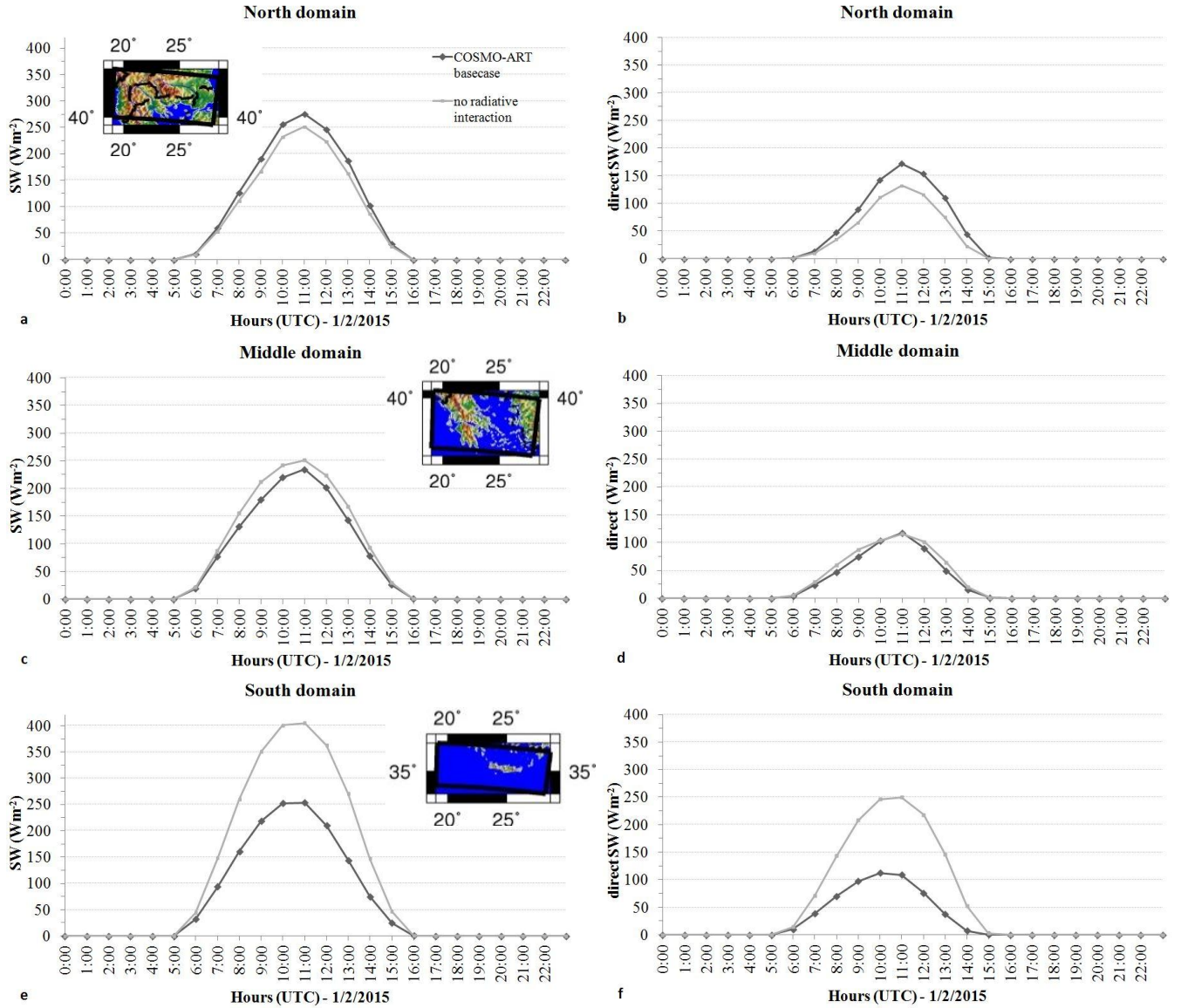
20

25

30

35

Figure 12: The diurnal variation of the GHI (a, c, e) and DNI (b, d, f) short-wave radiation zonally-averaged over the northern, middle and southern domains (maps shown). The dark grey line corresponds to the base-case COSMO-ART run that includes aerosol-meteorology. The light grey line corresponds to the scenario when aerosol-meteorology interaction is switched off.